JOURNAL OF PETROLOGY | VOLUME 47 | NUMBER 4 | PAGES 801–820 | 2006 | doi:10.1093/petrology/egi096

Cr-Saturation Arrays in Concentrate Garnet Compositions from Kimberlite and their Use in Mantle Barometry

HERMAN GRÜTTER[1]*, DEWETIA LATTI[1]† AND ANDREW MENZIES[2]

[1]DE BEERS CONSOLIDATED MINES LTD., P.O. BOX 82232, SOUTHDALE, 2135 SOUTH AFRICA

[2]MINERAL SERVICES SOUTH AFRICA, P.O. BOX 38668, PINELANDS, 7430 SOUTH AFRICA

RECEIVED DECEMBER 6, 2004; ACCEPTED NOVEMBER 30, 2005; ADVANCE ACCESS PUBLICATION JANUARY 4, 2006

The spinel–garnet transition in Cr/Al-enriched peridotitic bulk compositions is known from experimental investigations to occur at 20–70 kbar, within the pressure range sampled by kimberlites. We show that the Cr_2O_3–CaO compositions of concentrate garnets from kimberlite have maximum Cr/Ca arrays characterized by Cr_2O_3/CaO ~0·96–0·81, and interpret the arrays as primary evidence of chromite–garnet coexistence in Cr-rich harzburgitic or lherzolitic bulk compositions derived from depth within the lithosphere. Under Cr-saturated conditions on a known geotherm, each Cr/Ca array implicitly delineates an isobar inside a garnet Cr_2O_3–CaO diagram. This simplification invites a graphical approach to calibrate an empirical Cr/Ca-in-pyrope barometer. Carbonaceous chromite–garnet harzburgite xenoliths from the Roberts Victor kimberlite tightly bracket a graphite–diamond constraint (GDC) located at $Cr_2O_3 = 0{\cdot}94CaO + 5{\cdot}0$ (wt %), representing a pivotal calibration corresponding to 43 kbar on a 38 mW/m^2 conductive geotherm. Additional calibration points are established at 14, 17·4 and 59·1 kbar by judiciously projecting garnet compositions from simple-system experiments onto the same geotherm. The garnet Cr/Ca barometer is then simply formulated as follows (in wt %):

if $Cr_2O_3 \geq 0{\cdot}94CaO + 5$, then P_{38} (kbar) $= 26{\cdot}9 + 3{\cdot}22Cr_2O_3 - 3{\cdot}03CaO$, or

if $Cr_2O_3 < 0{\cdot}94CaO + 5$, then P_{38} (kbar) $= 9{\cdot}2 + 36[(Cr_2O_3 + 1{\cdot}6)/(CaO + 7{\cdot}02)]$.

*A small correction to P_{38} values, applicable for 35–48 mW/m^2 conductive geotherms, is derived empirically by requiring conventional thermobarometry results and garnet concentrate compositions to be consistent with the presence of diamonds in the Kyle Lake kimberlite and their absence in the Zero kimberlite. We discuss application of the P_{38} barometer to estimate (1) real pressures in the special case where chromite–garnet coexistence is known, (2) minimum pressures in the general case where Cr saturation is unknown, and (3) the maximum depth of depleted lithospheres, particularly those underlying Archaean cratons. A comparison with the P_{Cr} barometer of Ryan et al. (1996, Journal of Geophysical Research **101**, 5611–5625) shows agreement with P_{38} at 55 ± 2 kbar, and 6–12% higher P_{Cr} values at lower P_{38}. Because the P_{Cr} formulation systematically overestimates the 43 kbar value of the GDC by 2–6 kbar, we conclude that the empirical Cr/Ca-in-garnet barometer is preferred for all situations where conductive geotherms intersect the graphite–diamond equilibrium.*

KEY WORDS: *Cr-pyrope; chromite; P_{38} barometer; mantle petrology; lithosphere thickness*

INTRODUCTION

The aluminous phases in peridotitic rock types in the lithospheric upper mantle are well known from experimental evidence and xenolith studies to transform from plagioclase-facies to spinel-facies to garnet-facies with increasing pressure (Green & Ringwood, 1970; Harte & Hawkesworth, 1989). The subsolidus transition of spinel peridotite to garnet peridotite occurs via the generalized reaction pyroxene(s) + spinel = garnet + olivine and is located at pressures of ~16–20 kbar in Cr-free, Al-bearing peridotitic bulk compositions (MacGregor, 1965; O'Hara *et al.*, 1971; Robinson & Wood, 1998). At increasing peridotite Cr/(Cr + Al) ratios the reaction

*Corresponding author. Present address: BHP Billiton World Exploration Inc., Suite 800, Four Bentall Centre, 1055 Dunsmuir Street, Vancouver, B.C., V7X 1L2, Canada. Fax: +1 (604) 683-4125. E-mail: herman.grutter@bhpbilliton.com

†Present address: Rio Tinto Research and Technology Development, 1 Research Avenue, Bundoora 3083, Australia.

involves a multivariant pyroxene(s) + Cr-spinel + Cr-pyrope + olivine assemblage that progressively shifts the spinel–garnet transition to pressures as high as ~70 kbar, primarily as a result of strong partition of Cr into spinel relative to garnet (MacGregor, 1970; O'Neill, 1981; Klemme, 2004). The implied coexistence of Cr-spinel with Cr-pyrope garnet in depleted Cr/Al-enriched peridotitic bulk compositions has been confirmed by observation in kimberlite-borne xenoliths (e.g. Dawson *et al.*, 1978; Field & Haggerty, 1994; Schulze, 1996; Menzies, 2001) and in multiphase touching inclusions inside diamond (e.g. Sobolev *et al.*, 1976, 1997; Kopylova *et al.*, 1997). Early experimental results in the model MAS–Cr system (Malinovsky & Doroshev, 1975) showed that Cr-in-garnet isopleths have a weak negative dP/dT under Cr-saturated conditions, initiating the development of a promising Cr-in-garnet geobarometer by additional experimentation and related thermodynamic modelling (O'Neill, 1981; Irifune *et al.*, 1982; Chatterjee & Terhart, 1985; Irifune, 1985; Nickel, 1986; Webb & Wood, 1986; Doroshev *et al.*, 1997; Brey *et al.*, 1999; Girnis & Brey, 1999; Girnis *et al.*, 1999, 2003; Klemme & O'Neill, 2000; Klemme, 2004). Despite this effort, the few available thermodynamic calibrations of the Cr-in-garnet barometer have found little use in everyday mantle barometry, in part because they are mathematically complicated, but also because Cr–Al disequilibrium is often demonstrable in experimental charges and key uncertainties consequently remain regarding the stability of, and Cr–Al mixing in, high-temperature, high-pressure pyroxenes and garnet.

Semi-empirical Cr-in-pyrope thermobarometer models have nevertheless been calibrated for application to garnet compositions in heavy mineral concentrates derived from alkaline magmas such as kimberlite (Griffin & Ryan, 1995; Ryan *et al.*, 1996). The models are typically applied to a wide range of Cr-pyrope compositions and are commonly used in conjunction with Ni-in-garnet thermometry to constrain lithospheric geotherms at the time of kimberlite eruption (Ryan *et al.*, 1996; Tainton *et al.*, 1999; Griffin *et al.*, 2004). In these applications the coexistence of garnet with chromite is unknown and garnet compositions provide only an estimate of minimum pressure (Nickel, 1989; Griffin & Ryan, 1995). Similar semi-empirical Cr-based thermobarometers could, in principle, also be developed for orthopyroxene compositions (Nickel, 1989; Klemme & O'Neill, 2000), but the near-absence of orthopyroxene in kimberlitic heavy mineral concentrates would effectively curtail actual application. The Cr/(Cr + Al) ratio of clinopyroxene is a key ingredient of a recently developed thermobarometer applicable to garnet-facies lherzolitic clinopyroxene grains that commonly occur in kimberlitic heavy mineral concentrates (Nimis, 1998; Nimis & Taylor, 2000).

The objective of this study is documentation of chromite-saturation arrays defined by the Cr_2O_3–CaO compositions of xenocrystic Cr-pyrope garnets that occur in heavy mineral concentrates derived from kimberlite. A consequence of the straightforward empirical approach adopted here is the formulation of a simple, graphically intuitive minimum-pressure geobarometer that is valid for common harzburgitic and lherzolitic Cr-pyrope compositions. The barometer is calibrated using robust constraints provided by simple-system experimental results and the graphite–diamond equilibrium in natural chromite + garnet peridotite xenoliths, and requires only the garnet Cr_2O_3 and CaO content as input variables, plus an assumed geotherm. The work was inspired partly by 30–60 kbar isobars projected on a garnet Cr_2O_3–CaO diagram by Malinovsky & Doroshev (1977) and was initially developed to an extent similar to that presented here for Anglo American Research Laboratories (Pty.) Ltd. (AARL) by the two senior authors [unpublished work of Grütter and Smit (1994), but see Grütter (1994) and Grütter & Sweeney (2000)]. The simplicity of our empirical barometer suggests that it will be applied to a number of lithosphere-scale problems, and we discuss its use in situations involving real-pressure barometry, minimum-pressure barometry and base-of-lithosphere estimates. A brief comparison with the P_{Cr} barometer of Ryan *et al.* (1996) is also provided.

ANALYTICAL METHODS AND DATA SOURCES

A large proportion of the mineral compositions utilized in this work represent electron microprobe analyses for concentrate garnets prepared from samples of kimberlite. Most analyses were performed at AARL in Johannesburg, South Africa, in the mid-1980 s to early-1990s. An ARL electron microprobe equipped with nine wavelength-dispersive spectrometers was used and operated at an acceleration potential of 20 kV and a beam current of 30 nA. Counts were collected for 10 s on the K-α peak of all elements and background count levels estimated from long-term empirical trends. Standards comprised pure oxides MgO (Mg), Cr_2O_3 (Cr), Al_2O_3 (Al), TiO_2 (Ti) and Fe_2O_3 (Fe), as well as natural minerals rhodonite (Mn) and wollastonite (Ca,Si). Apparent concentrations were corrected for matrix effects with an online computer program (Bence & Albee, 1968). Lower limits of detection are calculated to be of the order of 0·06 wt % (at 2σ) for all elements. The calculated precision of CaO and Cr_2O_3 determinations is 2·5% relative (at 2σ), and was confirmed to be of that order by reanalysing the same spot 10, 25 and 100 times on an appropriate variety of garnet grains.

The AARL concentrate garnet compositions are augmented in certain instances with data provided by the

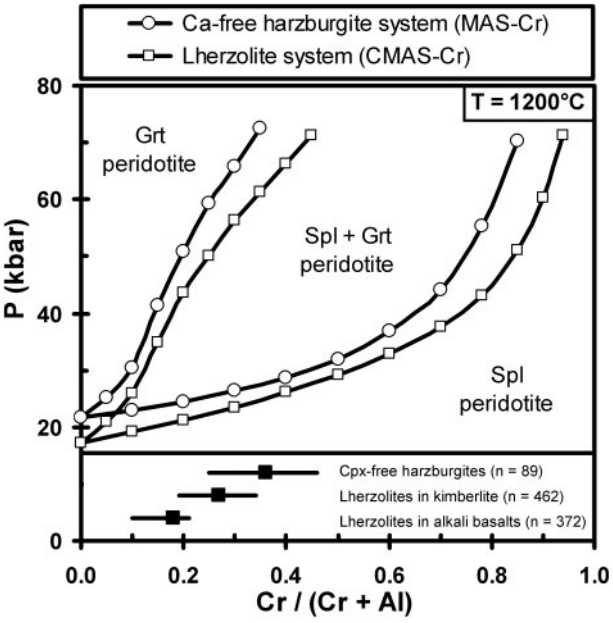

Fig. 1. Pressure–composition section at $T = 1200°C$ illustrating Cr/(Cr + Al) ratios of coexisting garnet (Grt) and spinel (Spl) in Fe-free model peridotite. Mineral compositions in lherzolite follow calculations by Webb & Wood (1986), modified at low Cr/(Cr + Al) to account for experimental garnets of Nickel (1986). Mineral compositions in Ca-free harzburgite follow the 1200°C experimental section of Irifune (1985). In Cr-free systems the spinel–garnet transition is univariant, occurring at 17·2 kbar in lherzolite and 21·7 kbar in Ca-free harzburgite (from Gasparik, 2000). The lower panel displays mean and inter-quartile ranges for Cr/(Cr + Al) in bulk-rock analyses of peridotite xenoliths from alkali basalts and kimberlites. (See text for discussion.)

Kimberlite Research Group (KRG) at the University of Cape Town. These, and ancillary compositional data for non-garnet species in peridotite xenoliths, were compiled from published literature and selected unpublished theses. Additional garnet Cr_2O_3–CaO values were also digitized from published diagrams using the freeware utility DataThief II. Appropriate reference is made in figure captions to identify and acknowledge various data sources.

USEFUL PRINCIPLES

P–T–X_{Cr} relations

The effect of pressure on Cr/(Cr + Al) in coexisting spinel and garnet in model lherzolite and Ca-free harzburgite lithologies is illustrated for fixed temperature in Fig. 1. Cr-spinel and garnet can coexist over a wide pressure interval for any given bulk peridotite Cr/(Cr + Al) ratio, and the mineral compositions show progressive Cr/Al enrichment to higher pressure. Garnet compositions in Ca-free harzburgites have ~20% lower Cr/(Cr + Al) than in lherzolites at any given pressure, implying that an equal-pressure tieline (an isobar) in a garnet Cr_2O_3 vs CaO diagram must show clear positive dependence on CaO. The barometer developed in this work takes advantage of this relationship. The P–X_{Cr} relations in Fig. 1 similarly predict that chromites in Ca-free chromite–garnet harzburgites have markedly lower Cr/(Cr + Al) than do chromites in chromite–garnet lherzolites, at any given pressure.

Garnet compositions in lherzolite xenoliths from alkali basalts are constrained by P, T and bulk Cr/(Cr + Al) ratios to have Cr/(Cr + Al) <0·2 (Fig. 1), which calculates to Cr_2O_3 <7·0 wt % based on the stoichiometry of pyropic garnet. That garnets in these xenoliths always contain significantly lower Cr_2O_3 (typically <3·0 wt % Cr_2O_3, Stern *et al.*, 1986; Ionov *et al.*, 1993) should be ascribed to low-pressure sampling of garnet-facies mantle by alkali basalts, or to the absence of garnet-saturated bulk compositions at depth. Higher bulk Cr/(Cr + Al) ratios in xenoliths from kimberlites permit garnet compositions to extend to Cr/(Cr + Al) ~0·35 (~12 wt % Cr_2O_3) in chromite-saturated lherzolite, and to Cr/(Cr + Al) ~0·45 (~16 wt % Cr_2O_3) in chromite-saturated Ca-free harzburgite (Fig. 1). Such Cr-rich pyropic garnet compositions are typically observed in concentrates from cratonic, diamond-bearing kimberlites (e.g. Gurney & Switzer, 1973; Sobolev *et al*, 1973), implying that chromite-saturated garnet peridotites may commonly occur at pressures inside the diamond stability field. This P–T–X_{Cr} relationship suggests that high-Cr concentrate garnets from diamondiferous kimberlites could display distinctive compositional evidence of chromite saturation. In what follows below, we identify such Cr-saturated compositional arrays as having garnet Cr_2O_3/CaO ~0·8–0·96 and use them as a cornerstone in the empirical calibration of our Cr/Ca-in-garnet barometer.

The compositions of coexisting Cr-pyrope garnet and chromite in model harzburgite systems (MAS–Cr ± Fe) have been examined experimentally at 900–1500°C at T/P conditions that fall above, or well above, the geothermal gradients characteristic of cratonic lithosphere (Fig. 2 and references therein). Attainment of Cr–Al equilibrium in garnet and pyroxene is an admitted problem, even at these high temperatures, and the experimental results currently permit considerable latitude in the P–T location of garnet Cr/(Cr + Al) isopleths (e.g. Girnis & Brey, 1999; Girnis *et al.*, 2003). Agreement does exist, however, that the $Cr/(Cr + Al)_{Grt}$ isopleths show weak to moderately negative dP/dT, such that the isopleths intersect common conductive lithospheric geotherms at a high angle and are predicted to show a regular increase of ~0·01$Cr/(Cr + Al)_{Grt}$ per kbar along (i.e. down) any given geotherm (Fig. 2). We capitalize on this fortuitous situation by explicitly choosing a model 38 mW/m^2 conductive geotherm (after Pollack & Chapman, 1977) as a mixed P–T standard

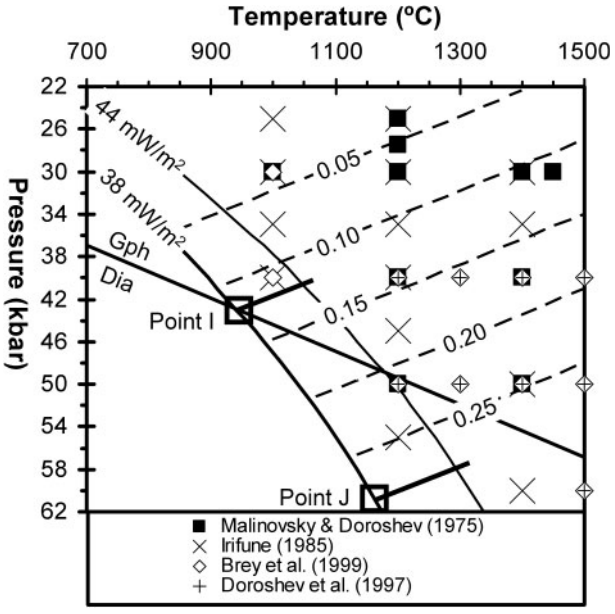

Fig. 2. Model conductive geotherms of 38 and 44 mW/m^2 (from Pollack & Chapman, 1977) in relation to the diamond stability field (Kennedy & Kennedy, 1976) and isopleths for pyrope–knorringite garnets in spinel-saturated MAS-Cr model harzburgite [dashed lines with labels denoting Cr/(Cr + Al)$_{Grt}$, from Malinovsky & Doroshev (1975)]. *P–T* conditions of other MAS-Cr experimental investigations are also shown. (See text for discussion, in particular for intersections labelled points I and J.)

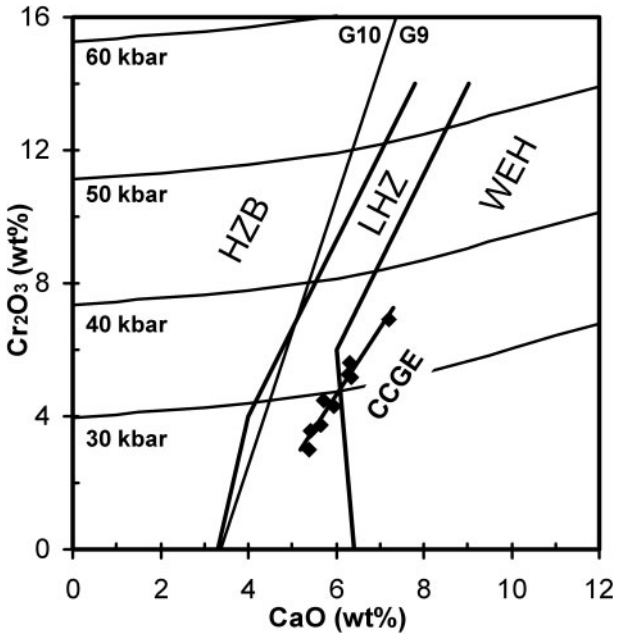

Fig. 3. Cr_2O_3 vs CaO diagram for peridotitic garnet. Compositional boundaries for garnets in harzburgite (HZB), lherzolite (LHZ) and wehrlite (WEH) assemblages are from Sobolev *et al.* (1973). Gurney (1984) determined that 85% of peridotitic garnets included in diamond fall to lower Ca than the G10–G9 boundary. The curved isobars demarcate pyrope–knorringite–grossular garnet compositions in chromite-saturated assemblages at 1200°C and pressures of 30–60 kbar (from Malinovsky & Doroshev, 1977). Refinement of these isobars is a prime objective of this study. The 'chromite–clinopyroxene–garnet equilibrium' (CCGE) trend from Jericho kimberlite xenoliths is also shown (from Kopylova *et al.*, 2000). (See text for discussion.)

state (Wood & Fraser, 1976) for our barometer. This 'unconventional' approach summarily simplifies the relationship of pressure with Cr/(Cr + Al)$_{Grt}$ in Cr-saturated systems and permits the use of a modest linear correction to reduce calculated pressures for hotter geotherms. As an illustration of the calibration procedure followed below, we note from Fig. 2 that the graphite–diamond transition intersects a 38 mW/m^2 geotherm at 43 kbar (Point I), corresponding to Cr/(Cr + Al)$_{Grt}$ ~0·12 based on the isopleths of Malinosky & Doroshev (1975). Conversely, the point labelled J occurs at Cr/(Cr + Al)$_{Grt}$ ~0·28 on a 38 mW/m^2 geotherm, which, for the isopleths illustrated, corresponds to P ~61 kbar. The same Cr/(Cr + Al)$_{Grt}$ would yield P ~58 kbar along a hotter 44 mW/m^2 geotherm.

The garnet Cr_2O_3–CaO diagram, Cr-saturated version

The garnet Cr_2O_3 vs CaO diagram (Fig. 3) is used globally by mantle petrologists and the diamond exploration community to represent the mineral compositions and assemblage of garnet-facies upper mantle peridotites, pyroxenites, eclogites and megacrysts (e.g. Gurney & Switzer, 1973; Sobolev *et al.*, 1973; Griffin *et al.*, 1999; Grütter *et al.*, 2004). Although denominated by only Cr_2O_3 and CaO, the diagram serves as a fairly comprehensive description of Cr-pyrope compositions because linear stoichiometric relations within the garnet formula $(Ca,Mg,Fe)_3(Al,Cr)_2Si_3O_{12}$ dictate that trivalent cation contents are completely specified by garnet Cr_2O_3 content, whereas divalent cation occupancy is specified by garnet CaO content and Mg/Fe ratio. Under the chromite-saturated conditions along a conductive geotherm that are of interest in this work, the diagram assumes special significance: if P is known from Cr/(Cr + Al)$_{Grt}$, then T is specified by the geotherm, and garnet Ca and Mg/Fe may be inverted to calculate the Mg/(Mg + Fe) of coexisting olivine and pyroxene using conventional Fe–Mg exchange thermobarometers (e.g. O'Neill & Wood, 1979; Harley, 1984). Cr/(Cr + Al)$_{Grt}$, P, T and calculated Fe–Mg site occupancy of pyroxene may then be used to estimate the tetrahedral Cr and Al contents of the coexisting orthopyroxene, although the parameters of the pyroxene solution model to be used are still being refined (Gasparik, 1987; Nickel, 1989; Klemme & O'Neill, 2000). The garnet P_{Cr} barometer of Ryan *et al.* (1996) uses an iterative inversion of this nature to construct a hypothetical orthopyroxene composition and

hence to solve the pressure of Cr saturation as a function of T and garnet composition. Our approach instead follows that of Malinovsky & Doroshev (1977) by developing the barometer empirically within the P–T–X projection plane represented by a garnet Cr_2O_3–CaO diagram and a geotherm implicitly specified by the Cr-saturated condition (see Fig. 3). Because small changes in bulk Mg/(Mg + Fe) do not materially affect Cr/Al partition between chromite, garnet and pyroxene (Brey *et al.*, 1999), we formulate our barometer without consideration of the small variations in Mg/Fe that occur in natural Cr-pyrope garnets.

Kopylova *et al.* (2000) described a 'chromite–clinopyroxene–garnet equilibrium' (CCGE) trend in comparatively rare orthopyroxene-absent spinel–garnet wehrlite assemblages derived from the low-temperature, low-pressure (650–850°C, 25–36 kbar) mantle underlying the Jericho kimberlite in northern Canada. Garnet compositions in the CCGE trend are moderately calcic and fall along a linear array with Cr_2O_3/CaO ~1·8, distinct from Cr_2O_3/CaO ~4·0 for a lherzolite assemblage (Kopylova *et al.*, 2000; Fig. 3). Similar linear CCGE-type compositional arrays have now been recognized in moderately calcic garnets from low-temperature (typically 700°C < T < 900°C) spinel–garnet wehrlite xenoliths in a number of kimberlite localities (Kopylova *et al.*, 2000, and references therein; Carbno & Canil, 2002; Lehtohnen *et al.*, 2004). These recent discoveries indicate that Cr-saturated garnet compositions are likely to define linear arrays within a garnet Cr_2O_3–CaO diagram and that Cr saturation at low garnet Cr_2O_3 content occurs at low pressure and low temperature on cool, cratonic geotherms. For instance, a garnet with 1·48 wt % Cr_2O_3 and 5·63 wt % CaO in a Jericho spinel–garnet lherzolite xenolith is calculated to derive from P–T (kbar–°C) of 14·4–520, 23·3–633, 26·7–690 or 31·8–781, based on conventional Al-in-opx thermobarometry [sample 22-1 of Kopylova *et al.* (1999)].

The graphite–diamond constraint (GDC)

Figure 4a portrays the Cr_2O_3–CaO compositions of garnets in graphite- or diamond-bearing peridotite xenoliths that also contain primary Cr-spinel. Additional data are available for diamond-bearing xenoliths without Cr-spinel (Fig. 4b) and graphite-bearing xenoliths without Cr-spinel (Fig. 4c). The mineral assemblage and compositional data for these xenoliths have been compiled (and often re-verified) from a large number of published and a few unpublished sources and are included as a supplementary dataset (Electronic Appendix 1, available at http://www.petrology.oxfordjournals.org). With a few notable exceptions, the mineral compositions are described as unzoned and similar data are reported for the same xenolith analysed at different facilities. Assemblages are internally consistent, except for sample A-90a, which is intensely serpentinized and has a low Cr/Ca garnet in a garnet + spinel + diamond assemblage (Sobolev *et al.*, 1984). As may be expected from the presence of diamond, the xenoliths are derived predominantly from economic or near-economic kimberlites located on cratons with cool, conductive geotherms (ranging from 36 to 41 mW/m^2; Finnerty & Boyd, 1987; Bell *et al.*, 2003; Griffin *et al.*, 2003). The localities represented are Finsch, Jagersfontein, the mines at Kimberley, Newlands, Premier, Roberts Victor, Star (all in South Africa), Letlhakane (in Botswana), Kao, Liqhobong, Mothae, Thaba Putsoa (in Lesotho), Aikhal, Dalnaya, Mir, Udachnaya (in Yakutia) and Schaffer-03 (in the USA).

With one exception in 148 available analyses the chromite-saturated garnet compositions show a remarkably consistent separation of graphite-bearing from diamond-bearing samples, indicating that minerals in these mantle samples attained Cr–Al and Ca–Fe–Mg equilibrium at the P–T conditions prevailing along common cratonic geotherms (Fig. 4a; Grütter, 1994). The division of graphite- from diamond-bearing samples is well constrained compositionally and, serendipitously, is defined by four xenoliths from the Roberts Victor locality—a Group-2 kimberlite situated in the central Kaapvaal craton. Acid-digestion residues of the four samples contain Cr-pyrope garnet, coarse euhedral Cr-spinel, graphite in samples RV160 and RV171, and diamond in samples RV175 and RV180 (Viljoen *et al.* 1994; K. S. Viljoen, personal communication, 1997). The garnet compositions hence define a unique chromite-saturated trend that transects the harzburgite compositional field in Cr_2O_3–CaO space (Fig. 4). We denote this relationship as the graphite–diamond constraint (henceforth the GDC) and describe it with the linear expression (in wt % oxides)

$$Cr_2O_3 = 0{\cdot}94CaO + 5{\cdot}0.$$

Significant variations in the position of the GDC as a function of Fe content are not expected because the Mg/(Mg + Fe) ratios of olivine in natural chromite–garnet harzburgite xenoliths is typically restricted to the range 0·93 ± 0·01 (e.g. Electronic Appendix 1). Other minor components, such as Fe_2O_3, TiO_2 and possibly MnO, could influence spinel–garnet relations in peridotites (MacGregor 1970; Fursenko, 1981; Woodland & O'Neill, 1995), but their relative variation in natural harzburgitic garnet compositions is evidently too small to cause noticeable displacement of the GDC in a Cr_2O_3–CaO diagram (Fig. 4a).

The P–T conditions of the GDC are, by mantle standards, reasonably well known. Garnets in graphite-bearing sample RV160 have the same Ni content as those in diamond-bearing sample RV175 (37 ± 3 ppm Ni, Viljoen *et al.*, 1994), implying that the two samples

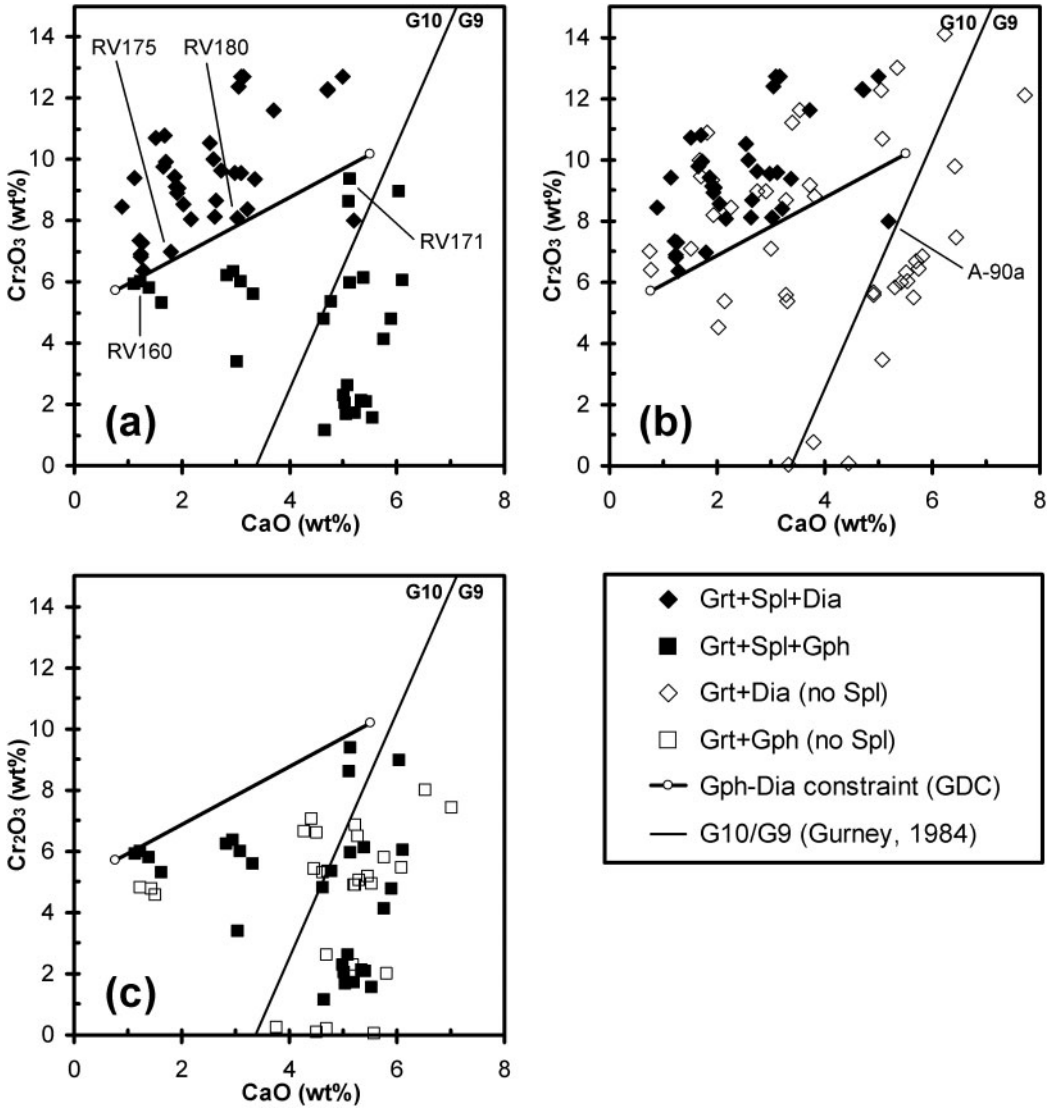

Fig. 4. Cr_2O_3–CaO compositions of garnet in spinel-saturated graphite- or diamond-bearing xenoliths (a), in diamond-bearing xenoliths, with or without spinel (b) and in graphite-bearing xenoliths, with or without spinel (c). Graphite in xenoliths RV160 and RV171 from Roberts Victor and diamond in RV175 and RV180 provide brackets for the graphite–diamond constraint (GDC). Sample A-90a has a low Cr/Ca garnet and represents the only inconsistency in 148 available analyses. Electronic Appendix 1 contains complete details of assemblages, mineral compositions and data sources.

bracket the graphite–diamond transition at the same mantle temperature, within error. This observation independently verifies the tight Cr–Ca constraints on the GDC (Fig. 4a) and pins the graphite–diamond transition at Roberts Victor at $T = 941 \pm 50°C$ [T_{Ni} calibration of Ryan *et al.* (1996)] and $P = 42{\cdot}9 \pm 1{\cdot}3$ kbar [on the graphite–diamond equilibrium of Kennedy & Kennedy (1976)]. Conventional thermobarometers place xenoliths from Group-2 kimberlites in the central Kaapvaal craton on a 38 mW/m^2 model conductive geotherm (Skinner, 1989; Menzies *et al.*, 1999; Menzies, 2001; Bell *et al.*, 2003), thereby corroborating an intersection with graphite–diamond at $P \sim 43$ kbar and $T \sim 940°C$ (Point I in Fig. 2). The unique P–T–X constraints provided by the GDC at Roberts Victor dictate calibration of our barometer at P–T conditions along a 38 mW/m^2 conductive geotherm, and a value of $P = 43$ kbar for graphite–diamond.

Cr-SATURATION ARRAYS IN CONCENTRATE GARNET COMPOSITIONS

Cr-pyrope garnets in heavy mineral concentrates derived from kimberlite occur as single, xenocrystic mineral

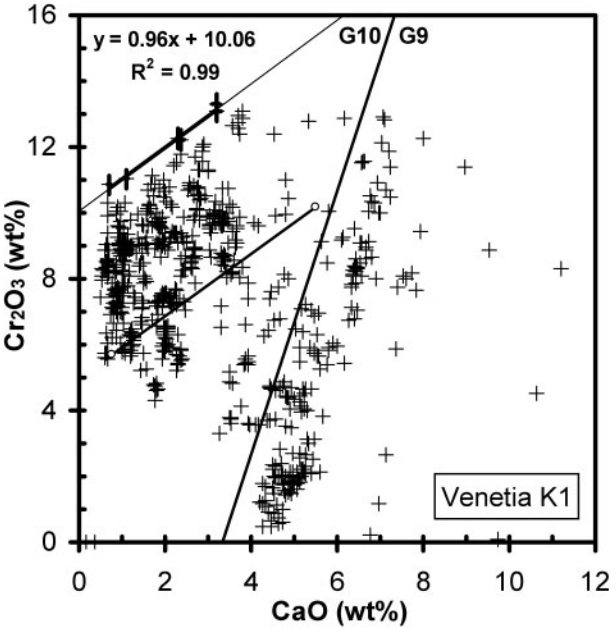

Fig. 5. Cr_2O_3–CaO compositions of concentrate garnets from the Venetia K1 kimberlite, Northern Province, South Africa (AARL, $n = 718$). In this and following figures, the compositions of Cr-rich garnets inferred to coexist with chromite are highlighted with ±2·5% relative errors and fitted with a linear regression (bold line segment and equation). Extrapolation of the regression (fine line) facilitates comparison with all available data and the GDC (fine line with open circles, as in Fig. 4). The G10–G9 boundary is that of Gurney (1984).

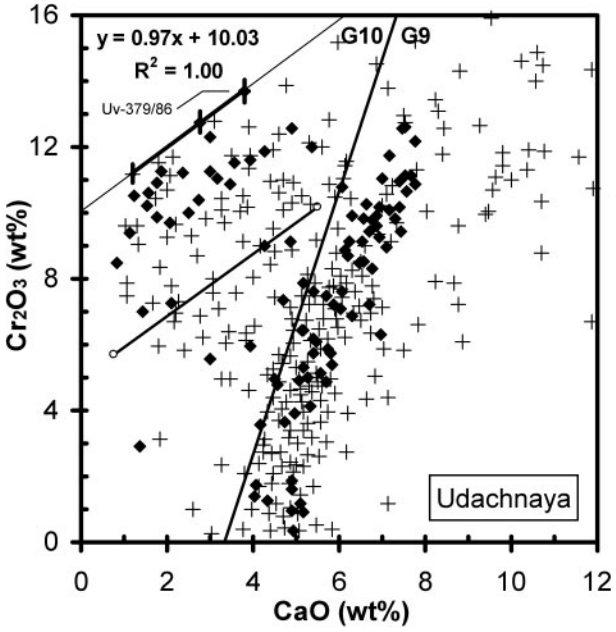

Fig. 6. Cr_2O_3–CaO compositions of garnets in concentrate (crosses, $n = 292$) and in peridotite xenoliths (filled diamonds, $n = 101$) from the Udachnaya kimberlite, Yakutia. Note the presence of garnets with Cr_2O_3 >14 wt % at moderate to high CaO and compare with Venetia K1 data given in Fig. 5. Xenolith Uv-379/86 contains primary chromite coexisting with high-Cr garnet (Griffin *et al.*, 1993). Data reproduced from Sobolev *et al.* (1973, fig. 1) and Sobolev *et al.* (1993, fig. 2).

grains disaggregated from their host rock and their paragenesis is formally unknown. Although derivation from wehrlitic, lherzolitic or harzburgitic assemblages can be inferred from garnet Ca-saturation characteristics (e.g. Schulze, 1995; Fig. 3), the Cr-saturation status of a xenocryst garnet cannot be determined. We consequently apply a limiting approach to identify concentrate garnets that may have coexisted with chromite—for a large number of grains analysed from a single kimberlite intrusion, those most likely to be Cr saturated have the highest Cr content at any given Ca content.

Application of this concept to concentrate garnet compositions from the Venetia K1 kimberlite highlights the presence of six high-Cr garnets with variable Ca that occur on a linear array with Cr_2O_3/CaO slope near unity (Fig. 5). Although the compositional array is poorly constrained at Cr_2O_3 >13·5 wt % by the absence of high-Cr garnets with moderate Ca, it nevertheless defines a limiting Cr-content envelope for low-Ca garnet compositions. Garnets with higher Cr do not occur in a database of over 5000 analyses representing concentrate from all of the 11 known Venetia kimberlites (De Beers, unpublished data, 2004). The six grains highlighted in Fig. 5 are thus the most Cr-rich of all peridotitic garnets contained within the Venetia kimberlite province; their alignment along a linear array falling essentially parallel to the GDC is considered exceptionally strong evidence in support of chromite-saturated conditions at high garnet Cr content, and thus at pressures well in excess of the GDC.

The upper Cr limit for peridotitic garnets from the Udachnaya kimberlite is essentially coincident with that at Venetia. A significant range of Ca is recorded in high-Cr garnets from Udachnaya and the upper Cr limit is constrained to be subparallel to the GDC and linear, or approximately so, over the full range of Ca possible in harzburgitic garnet compositions (Fig. 6). Concentrate garnets account for two of three high-Cr data points from Udachnaya—the third represents harzburgite xenolith Uv-379/86 in which high-Cr primary chromite coexists with high-Cr garnet (Griffin *et al.*, 1993). This relationship affirms chromite saturation as the cause of arrays with Cr_2O_3/CaO ∼0·96 that delimit concentrate garnet compositions from Venetia and Udachnaya. The Cr-saturated arrays for both kimberlites intercept the Ca-free axis at ∼10·0 wt % Cr_2O_3 (Figs 5 and 6), which recalculates to $Cr/(Cr + Al)_{Grt}$ ∼0·28 and represents an extreme high-pressure calibration point for our barometer (labelled point J in Fig. 2).

Concentrate from the Finsch kimberlite contains many low-Ca garnets with elevated Cr content. The compositions of six high-Cr grains fall within analytical error of

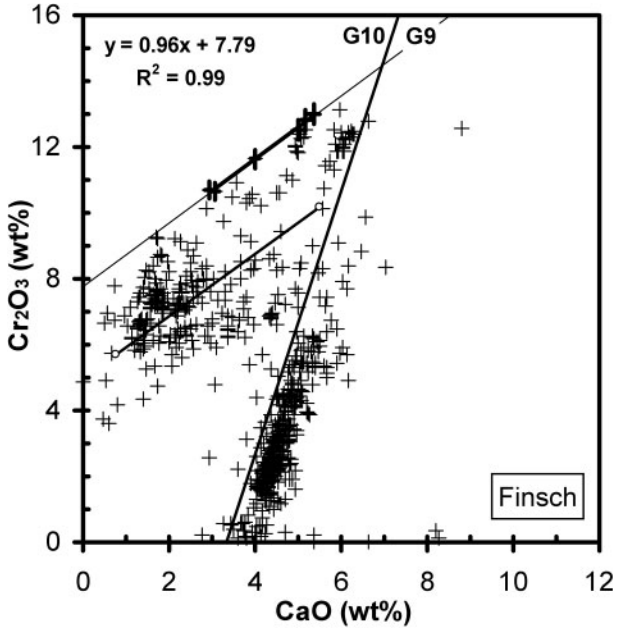

Fig. 7. Cr_2O_3–CaO compositions of garnets in concentrate from the Finsch kimberlite, Northwest Province, South Africa (AARL, $n = 664$). The limiting Cr-saturation array is well defined by six harzburgitic garnets with the highest Cr content at any given Ca content. (See text for discussion.)

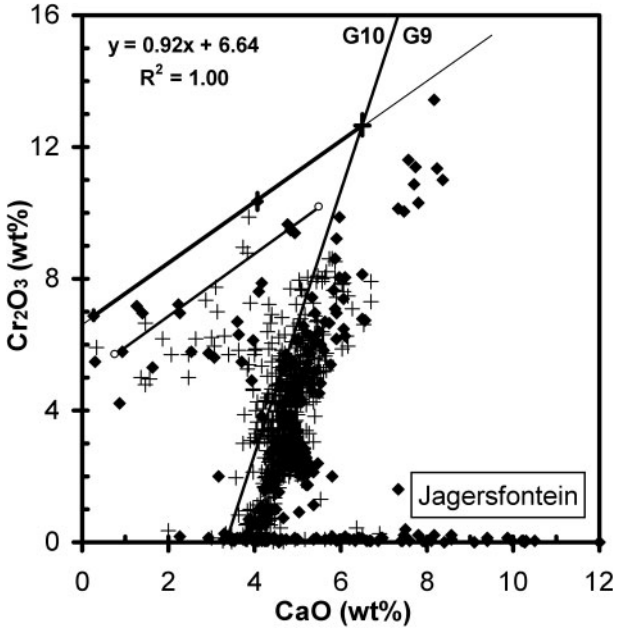

Fig. 8. Cr_2O_3–CaO compositions of garnets in concentrate (crosses) and in peridotite xenoliths (filled diamonds) from the Jagersfontein kimberlite, South Africa. The indicated Cr-saturation array is fitted to three garnets with a wide range in Ca content. Concentrate garnet data are from the AARL ($n = 477$), the KRG ($n = 88$) and D. J. Schulze ($n = 101$, personal communication). Xenolith data are from the KRG ($n = 152$), numerous published and a few unpublished sources ($n = 208$, including many eclogitic garnets), and reproduced from Burgess & Harte (1999, fig. 2, $n = 74$). A total of 895 analyses have $Cr_2O_3 > 1{\cdot}0$ wt %. (See text for discussion.)

a linear array formulated as $Cr_2O_3 = 0{\cdot}96CaO + 7{\cdot}79$ (in wt %) which parallels the GDC, but at 2·79 wt % higher Cr_2O_3 content (Fig. 7). We interpret the array as demarcating Cr-saturated conditions at a pressure higher than the GDC, but less than at Udachnaya. High-Cr lherzolitic garnets are exceptionally rare at Finsch when compared with Venetia and Udachnaya (see Figs 5, 6 and 7), implying that chromite-saturated garnet lherzolite xenoliths may be a rarity at Finsch. Low- to moderate-Cr garnet lherzolite xenoliths are common at Finsch and, although derived from high pressure on a 38 mW/m^2 geotherm (53–62 kbar at 1100–1250°C), none are reported to contain primary Cr-spinel (Gurney & Switzer, 1973; Shee *et al.*, 1982; Skinner, 1989; Bell *et al.*, 2003). In contrast to high-Cr garnet harzburgites, the Finsch garnet lherzolites apparently have bulk Cr/(Cr + Al) ratios too low to stabilize chromite at high pressure and temperatures of ~1200°C (see Fig. 1).

Peridotitic garnets derived from concentrate or xenoliths from the Jagersfontein kimberlite commonly have moderate to low Cr contents, and only a small proportion have Cr contents higher than the GDC (~1·7%; see Fig. 8). Three such grains span the Ca content range of the entire harzburgite compositional field and align perfectly in an array parallel to the GDC that we interpret as resulting from chromite saturation. That the interpreted Cr-saturation array represents a limiting upper envelope is supported by three additional analyses, also spanning a large Ca range, which fall outside analytical error at marginally lower Cr content (Fig. 8).

Lherzolitic compositions dominate the concentrate garnets derived from the Koffiefontein kimberlite, and all of these fall to lower Cr than a Cr-saturation array defined by three of the few harzburgitic garnets recovered at this locality (Fig. 9). The Koffiefontein Cr-saturation array is coincident with the GDC within analytical error. Peridotitic garnets included in Koffiefontein diamonds overlap to lower Ca the compositions of harzburgitic concentrate garnets, at Cr/Ca contents similar to or lower than the GDC (Fig. 9). This apparent contradiction of the GDC is explicable by the absence of chromite coexisting with garnet in the described diamond-inclusions (Rickard *et al.*, 1986; Griffin *et al.*, 1992). Making the reasonable assumption that a typically cratonic geotherm pertains, the concentrate data locate chromite–garnet harzburgites at the GDC (i.e. at the graphite–diamond transition) in the Koffiefontein lithosphere, whereas the diamond-inclusions relate to chromite-free garnet–diamond harzburgites derived from within the diamond stability field. Apart from the occurrence of diamond itself, the presence of diamond-facies harzburgite at Koffiefontein is forecast by a single very

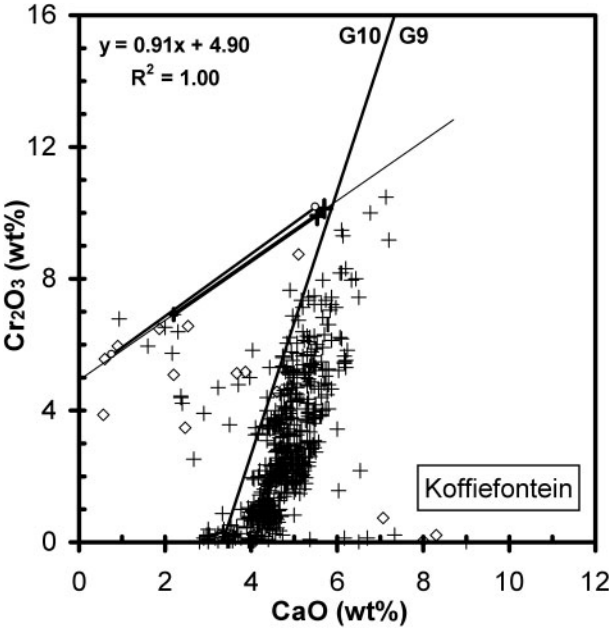

Fig. 9. Cr_2O_3–CaO compositions of garnets in concentrate (crosses) and included in diamonds (open diamonds) from the Koffiefontein kimberlite, South Africa. The indicated Cr-saturation array is fitted to three concentrate garnet compositions and falls within analytical error of the GDC. (See text for an interpretation of these data.) Concentrate compositions are from the AARL ($n = 519$) and the KRG ($n = 484$). The compositions of garnets occluded by diamond are from Rickard *et al.* (1986, $n = 14$) and Griffin *et al.* (1992, $n = 7$).

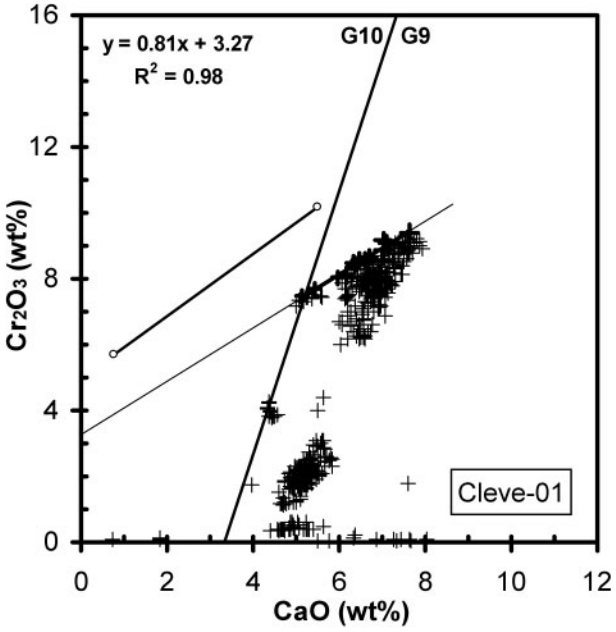

Fig. 10. Cr_2O_3–CaO compositions of concentrate garnets from the non-diamondiferous Cleve-01 kimberlite, Eyre Peninsula, South Australia. The indicated Cr-saturation array is fitted to the 13 highest Cr garnets at given Ca. (See text for discussion.) Analyses are those of Wyatt *et al.* (1994, fig. 4, $n = 582$, kindly provided on request).

low-Ca concentrate garnet with Cr_2O_3 ~0·9 wt % higher than the GDC (see Fig. 9). We discuss the significance of such compositionally isolated high-Cr/Ca analyses further below.

Concentrate garnets from the Cleve-01 kimberlite show clear truncation of Cr-rich lherzolitic compositions at a Cr_2O_3/CaO slope similar to the GDC (Fig. 10). However, a line fitted to all the highest Cr data at given Ca produces a Cr-saturation array with a slope subtly shallower than the GDC (Fig. 10). The difference in slope is considered robust, as omission of any one, two or three randomly selected high-Cr data points fails to produce fitted lines with a Cr_2O_3/CaO slope higher than or equal to the GDC. Wyatt *et al.* (1994) postulated the geotherm at Cleve-01 to be close to cratonic and related its lack of diamonds to a gravitational settling event that occurred during transit of the kimberlite magma through the uppermost mantle. This explanation is considered implausible given the presence of common 0·3–2·0 mm sized mantle-derived ilmenite, chromite, garnet and chromian diopside in the kimberlite, raising the prospects that diamond-hosting lithologies may have been absent from the lithosphere sampled by Cleve-01, or that the kimberlite magma entrained mantle materials from within the graphite stability field only. The latter interpretation is supported by the presence of a Cr-saturated array at Cr contents appreciably below the GDC and by the absence of xenocryst garnets with Cr content higher than the GDC.

The compositions of garnets overlying the Nzega kimberlite in Tanzania are shown in Fig. 11. Roughly 75% of the garnets record $750°C < T_{Ni} < 800°C$, placing them in a narrow temperature interval some 165°C lower than the GDC and well inside the graphite stability field on the ~37 mW/m^2 model conductive geotherm established for the locality (see Tainton *et al.*, 1999). The coexistence of chromite with garnet over such a narrow and low-temperature interval is expected to produce a well-constrained Cr-saturation array displaced to appreciably lower Cr content than the GDC. An appropriately situated Cr-saturation array is defined for Nzega by six garnets with Ca contents covering low-Ca harzburgitic to Ca-rich lherzolitic compositions (Fig. 11). The array is noted to have a slope similar to that at Cleve-01, and subtly different from the GDC.

Garnet lherzolite and spinel–garnet lherzolite xenoliths are infrequently observed together with abundant spinel peridotite xenoliths in alkali basalt vents. The compositions of garnets from alkali basalts should logically also show Cr-saturation arrays, and two examples are given here (Figs 12 and 13). The Cr-saturation arrays in both instances slope at Cr_2O_3/CaO ~0·27, whether interpreted for numerous concentrate garnet compositions from Tieling, China (Fig. 12), or for lesser amounts of

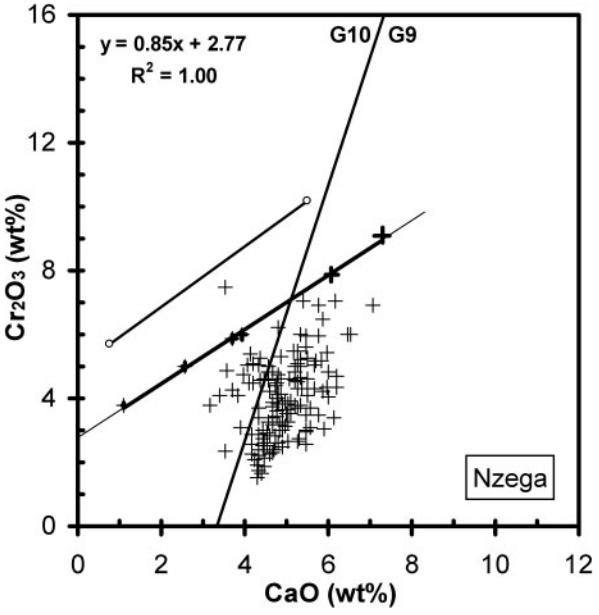

Fig. 11. Cr_2O_3–CaO compositions of garnets from tightly spaced grid loam samples overlying the Nzega kimberlite, Tanzania [143 data points reproduced from Tainton *et al.* (1999, fig. 9)]. (See text for discussion.)

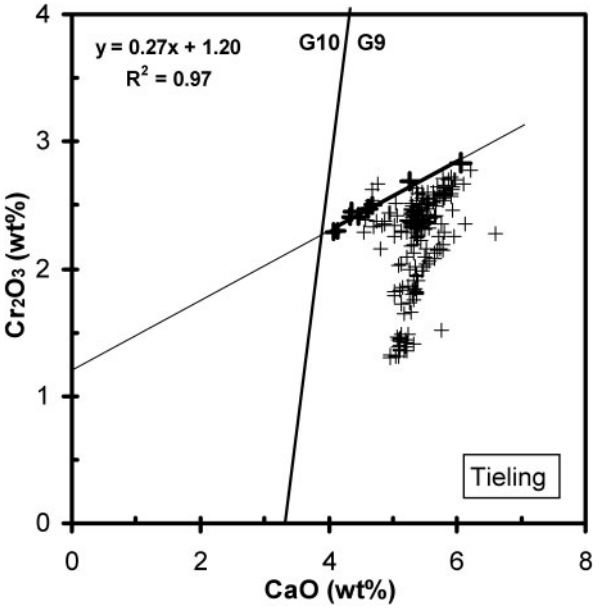

Fig. 12. Cr_2O_3–CaO compositions of concentrate garnets from alkali basalt vents near Tieling, northeastern Liaoning province, China (AARL, $n = 239$). The interpreted Cr saturation is fitted to nine data points. (See text for discussion.)

data representing spinel–garnet lherzolite xenoliths from Pali-Aike, Chile (Fig. 13). The marked change in slope relative to the GDC is a consequence of the decreased separation between 'garnet-in' curves for lherzolite and harzburgite at lower pressures (see Fig. 1). The effect is

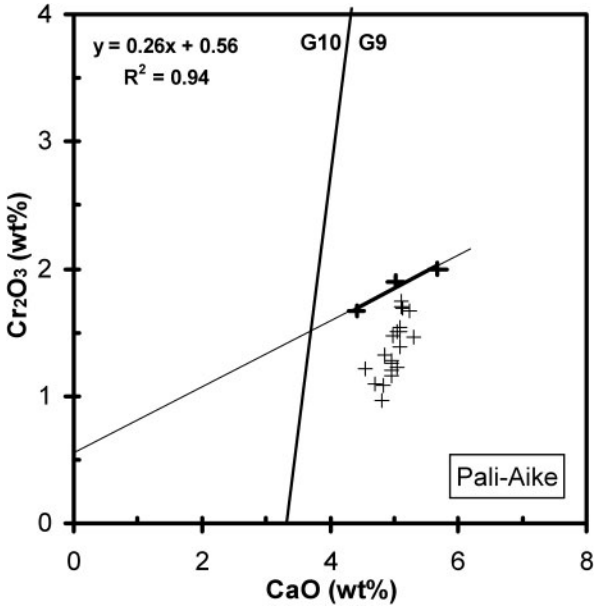

Fig. 13. Cr_2O_3–CaO compositions of 23 garnets in lherzolite xenoliths from the Pali-Aike alkali basalts, southern Chile. The three highest Cr garnets are known to coexist with Cr-spinel. Data from Skewes & Stern (1979), Smith & Wilson (1985) and Stern *et al.* (1986). (See text for discussion.)

particularly noticeable in fertile, Cr/Al-poor bulk compositions and consequently affects formulation of our empirical Cr/Ca-in-garnet barometer for low-Cr garnet compositions.

CALIBRATION OF A SIMPLE BAROMETER

When collated as a family of lines, the Cr-saturation arrays outlined above form a simple graphical template that may be used to formulate an empirical barometer, valid for common harzburgitic and lherzolitic garnet compositions derived from kimberlite (Fig. 14). Arrays richer in Cr than the GDC may be visualized as falling parallel to the GDC and differing from one another only by the value of their ordinate within line segment I–J. Arrays poorer in Cr than the GDC are related to one another by differences in slope and in ordinate values. A rotation about a point located near $-1{\cdot}5$ wt % Cr_2O_3 and $-7{\cdot}0$ wt % CaO would serve to describe them. Calibration of the barometer requires a mathematical description of these highly intuitive graphical attributes, as well as established pressure values for garnet compositions near the extremities of the area of interest (points labelled L, H, I and J in Fig. 14). We hence proceed by finding pressures referenced to our chosen standard-state 38 mW/m^2 model conductive geotherm for spinel-saturated garnet compositions corresponding to points L, H, I and J.

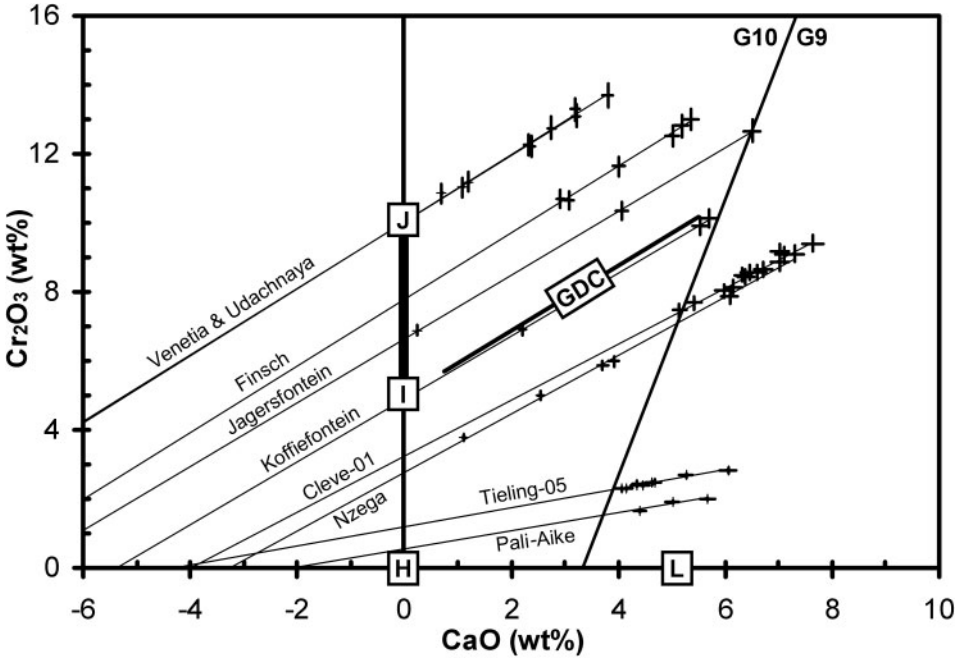

Fig. 14. Summary of fitted Cr-saturation arrays from the kimberlites indicated. The array family serves as a graphical template for development of an empirical Cr/Ca-in-garnet barometer, which is underpinned by pressure calibration points at compositions marked by L, H, the GDC and line segment I–J. (See text for discussion.)

Table 1: Summary of experimental data in Cr-bearing peridotitic systems

Result	System	T (°C)	P at J* (kbar)	P at I* (kbar)	ΔP J–I*† (kbar)	dP/dT (bar/°C)	Reference
1	MAS-Cr	1200	58·9	39·9	19·0	−24·0	Malinovsky & Doroshev (1975)
2	MAS-Cr	1200	58·8	39·8	19·0	−24·3	Malinovsky & Doroshev (1977)
3	MAS-Cr	1200	60·6	37·1	23·5		Irifune (1985)
4	MAS-Cr	1200	50·9	31·4	19·5	−44·0	Brey *et al*. (1991)
5	MAS-Cr	1200	51·6	33·2	18·4	−31·3	Doroshev *et al*. (1997)
6	FMAS-Cr‡	1200	53·3	39·0	14·3	−54·9	Girnis & Brey (1999)
7	CMAS-Cr‡					−33·1	Nickel (1986)

*J occurs at XCr,Grt = 0·28 and I occurs at XCr,Grt = 0·14 in a Ca-free system.
†ΔP J–I averages 19·0 ± 2·9 kbar for all results (1–6) and 19·0 ± 0·4 kbar omitting results 3 and 6.
‡F is Fe; M, Mg; C, Ca; A, Al; S, Si.

Point L in Fig. 14 represents a garnet in a fertile, Cr-free lherzolite that would be in equilibrium with Fo_{90} olivine, two pyroxenes and Al-spinel at P = 14·0 kbar and T ~390°C on a 38 mW/m^2 geotherm [based on the CMAS model of Gasparik (2000) with an Fe correction from O'Neill (1981)]. Garnet composition H occurs on the same geotherm at P = 17·4 kbar and T ~470°C in a Cr-free harzburgite assemblage with Fo_{90} olivine, enstatite and Al-spinel (based on the same model as above). Point I occurs at Cr/(Cr + Al)$_{Grt}$ = 0·14 in a depleted Ca-free, Cr-enriched harzburgite–dunite assemblage with Fo_{93} olivine and high-Cr spinel. Point I assumes P–T values of the GDC (P = 43 kbar at T ~940°C) on a 38 mW/m^2 geotherm, as outlined above.

Point J occurs at Cr/(Cr + Al)$_{Grt}$ = 0·28, corresponding to the highest Cr concentrate garnet from kimberlite that would coexist with chromite in a Ca-free chromite–garnet harzburgite–dunite assemblage with Fo_{93} or Fo_{94} olivine. Current experimental results at 1200°C yield pressures of ~51 to ~61 kbar for J (Table 1, Fig. 2), representing a range too large to use in our calibration. However, we note the isothermal pressure difference between J and I averages 19·0 ± 2·9 kbar across six

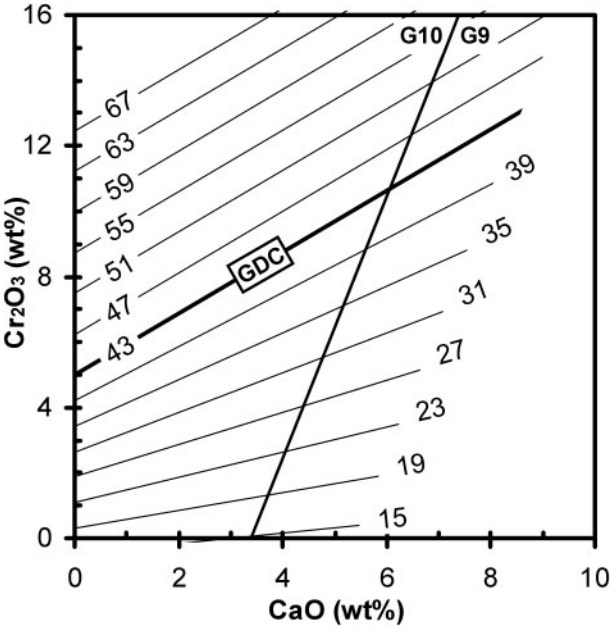

Fig. 15. Cr_2O_3 vs CaO diagram for mantle-derived peridotitic garnet with superimposed isobars (in kbar) according to the P_{38} barometer formulation. The GDC assumes a value of 43 kbar. (Compare with Fig. 3 and see text for discussion.)

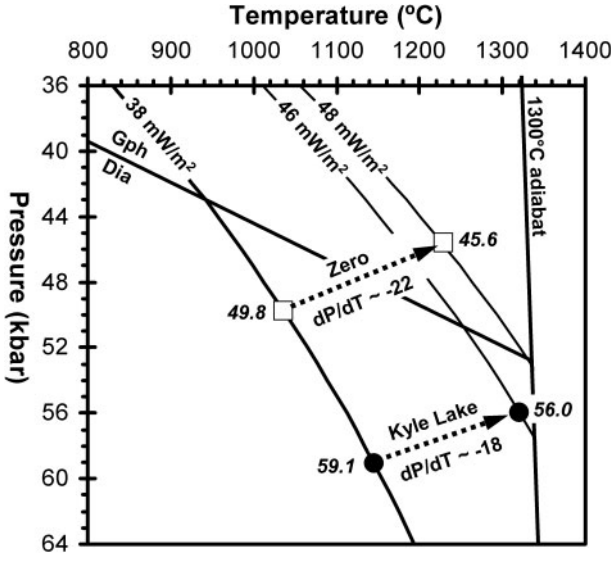

Fig. 16. *P–T* relations for 38, 46 and 48 mW/m^2 conductive model geotherms, the graphite–diamond equilibrium (Kennedy & Kennedy, 1976) and a mantle adiabat. Dashed arrows indicate apparent displacement of the deepest mantle materials in the Zero and Kyle Lake kimberlites, for geotherms substantially hotter than a 38 mW/m^2 model. (See text for discussion.)

separate experimental investigations (or 19·0 ± 0·4 kbar omitting two outliers; Table 1), implying that J occurs at roughly 19 kbar higher pressure than the GDC (from Fig. 14). By applying a small pressure reduction to account for the temperature difference between J and I along a 38 mW/m^2 geotherm (Fig. 2), we estimate that point J occurs at $P \sim 59{\cdot}1$ kbar and $T \sim 1150°C$.

The barometer is then formulated (in wt % oxides and kbar) as follows:

if $Cr_2O_3 \geq 0{\cdot}94CaO + 5$, then $P_{38} = 26{\cdot}9 + 3{\cdot}22Cr_2O_3 - 3{\cdot}03CaO$, or
if $Cr_2O_3 < 0{\cdot}94CaO + 5$, then $P_{38} = 9{\cdot}2 + 36[(Cr_2O_3 + 1{\cdot}6)/(CaO + 7{\cdot}02)]$

where the subscript explicitly specifies the reference 38 mW/m^2 model conductive geotherm (as shown in Fig. 2). Figure 15 shows a graphical representation of isobars defined by the formulation. The calibration is not valid for wehrlitic garnet compositions because their chromite-saturation arrays appear to fall along trends at high angles to those in harzburgites and lherzolites (see CCGE trend in Fig. 3).

Pressures calculated with the P_{38} formulation have to be reduced for geotherms hotter than the 38 mW/m^2 reference state because garnet Cr-content isopleths in chromite-saturated model harzburgite and lherzolite compositions have negative dP/dT (e.g. Fig. 2). Because the magnitude of the correction is poorly known (–24 to −55 bar/°C, Table 1), we construct an empirical correction based on mantle materials from the Zero and Kyle Lake kimberlites, which have elevated geotherms. Ca-poor Cr-pyrope xenocrysts from the Zero kimberlite, South Africa, provide P_{38} pressures up to 49·8 kbar, but thermobarometry on peridotite xenoliths (Shee *et al.*, 1989) and clinopyroxene xenocrysts (using Nimis & Taylor, 2000) limits actual pressures to 45·6 kbar on a 48 mW/m^2 conductive geotherm. Such a geotherm barely intersects the diamond stability field (Fig. 16), consistent with the absence of diamond at Zero. The Kyle Lake kimberlites in Ontario, Canada, contain Ca-poor, high-Cr garnets (Sage, 2000) with P_{38} values up to 59·1 kbar. Clinopyroxene thermobarometry constrains actual pressures up to 56·0 kbar, at high temperatures in the diamond stability field on a 46 mW/m^2 geotherm (Fig. 16). The Kyle Lake kimberlites contain numerous brown-tinted and graphite-coated diamonds, features that are considered consistent with deformation and/or residence of the diamonds at high mantle temperatures (Harris, 1992). The 48 mW/m^2 and 46 mW/m^2 conductive geotherms for Zero and Kyle Lake adequately account for the occurrence and state of diamonds in the kimberlites, and for the two localities combined indicate dP/dT of garnet Cr-content isopleths to be approximately −20 bar/°C (dashed arrows in Fig. 16). Our empirical barometer thus includes a small pressure correction for variable geothermal

Table 2: Pressure estimates for Cr-rich garnets in concentrate from kimberlite

Locality	Cr_2O_3 (wt %)	CaO (wt %)	Reference	P_{38} (kbar)	Notes
Real-pressure estimates (chromite-saturated)					
Venetia	13·29	3·19	Fig. 5	60·0	$P_{35} = 61·1$ kbar
Udachnaya	12·76	2·75	Fig. 6	59·7	$P_{35} = 60·8$ kbar
Finsch	13·0	5·36	Fig. 7	52·5	1 of 3 at this P_{38}
Finsch	12·81	5·18	Fig. 7	52·5	2 of 3 at this P_{38}
Finsch	10·7	2·92	Fig. 7	52·5	3 of 3 at this P_{38}
Jagersfontein	6·89	0·25	Fig. 8	48·3	$P_{40} = 47·5$ kbar
Koffiefontein	10·14	5·71	Fig. 9	42·4	$P_{40} = 41·7$ kbar
Koffiefontein	6·91	2·2	Fig. 9	42·4	$P_{40} = 41·7$ kbar
Cleve-01	9·16	7·02	Fig. 10	36·8	$P_{40} = 36·1$ kbar
Kyle Lake	12·05	2·19	Fig. 16	59·1	$P_{46} = 56·0$ kbar
Zero	9·72	2·77	Fig. 16	49·8	$P_{48} = 45·9$ kbar
Minimum-pressure estimates (chromite coexistence unknown)					
Roberts Victor*	10·53	2·53	RV177*	$\geq$53·1	Type locality for P_{38} model
Koffiefontein	6·77	0·93	Fig. 9	$\geq$45·9	$P_{40} \geq 45·1$ kbar
Nzega	7·49	3·52	Fig. 11	$\geq$34·3	$P_{37} \geq 34·7$ kbar
Portage	12·83	2·09	Fig. 17	$\geq$61·9	P_{38} model assumed
Beaver Lake	10·25	5·98	Fig. 17	$\geq$42·0	P_{38} model assumed

*Garnet in xenolith RV177 (Stachel *et al.*, 1998).

gradients, which is expressed (in kbar) in simplified linear format as

$$P_{CG} = 0·997P_{38} - 0·388CG + 14·9$$

where CG denotes a model conductive geotherm [in mW/m^2, after Pollack & Chapman (1977)]. Substituting for Zero, we compute $P_{38} = 49·8$ kbar to be equivalent to $P_{48} = 45·9$ kbar. It is worth noting that a typical convective mantle adiabat intersects the graphite–diamond equilibrium at high temperature on a 48 mW/m^2 geotherm (Fig. 16). As our barometer is calibrated to be consistent with conductive geotherms that intersect the graphite–diamond equilibrium, we caution against its application where this is not the case (Fig. 16).

APPLICATIONS AND DISCUSSION

Because of its inherent mathematical simplicity, formulation in terms of only two oxide-denominated variables and comparatively low temperature dependence, the barometer presented in this work may be applied in several situations where Cr-pyrope garnets occur. Here we discuss application to garnet compositions for (1) the special case where garnet–chromite coexistence can be demonstrated, (2) the general case where chromite coexistence with garnet is indeterminate, and (3) base-of-lithosphere depth estimates. A brief comparison is also made with the P_{Cr} barometer of Ryan *et al.* (1996).

Chromite-present (real-pressure) barometry

The empirical approach taken to construct our barometer required special selections to be made of kimberlite-derived garnet concentrate data, which emphasize the presence of chromite-saturated compositional arrays (Figs 5–13 and summary in Fig. 14). The barometer yields a real-pressure estimate under such Cr-saturated conditions, and appropriate calculated values for selected garnet compositions are listed in Table 2.

Given that the highest Cr/Ca garnets at Venetia and Udachnaya coexist with chromite (Figs 5 and 6), we estimate $P_{38} \sim 60$ kbar for them, and $P_{35} \sim 61$ kbar for the 35 mW/m^2 conductive geotherms established by conventional thermobarometry at these localities (Griffin *et al.*, 1996; Stiefenhofer *et al.*, 1999). Identical real-pressures of $P_{38} = 52·5$ kbar are calculated for three of six chromite-saturated high-Cr/Ca harzburgitic garnets from Finsch (Fig. 7), even though their Cr_2O_3 and CaO contents differ considerably (Table 2). The pressures calculated for garnets from Venetia, Udachnaya and Finsch are well in excess of that required for diamond to be present at these localities, implying that these kimberlites have entrained depleted, Cr/Al-enriched garnet

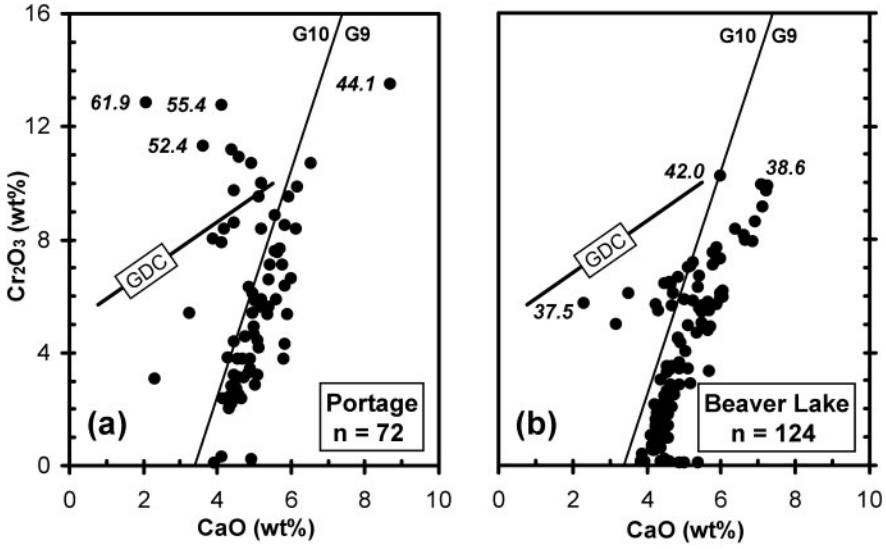

Fig. 17. Cr_2O_3–CaO data for garnets from the Portage area (a) and the Beaver Lake kimberlite (b) which are separated by ~90 km in central Quebec, Canada. Bold italics indicate P_{38} model pressures for selected compositions. Data for Portage reproduced from the website of Majescor Resources (http://www.majescor.com). The Beaver Lake data are from Girard (2001). (See text for discussion.)

peridotite over a considerable depth range from within the diamond stability field.

The geotherm applicable to Group-1 kimberlites on the Kaapvaal craton is well known to follow a 40 mW/m^2 conductive model, marginally hotter than the 38 mW/m^2 geotherm of Group-2 kimberlites (Finnerty & Boyd, 1987; Bell *et al.*, 2003). We accordingly calculate P_{40} pressures of 47·7 and 41·9 kbar for chromite-saturated harzburgitic garnets from the Jagersfontein and Koffiefontein kimberlites, respectively. Table 2 shows the difference between P_{40} and P_{38} estimates to be rather small, indicating that either model could be applied to garnet compositions from Kaapvaal kimberlites without incurring perceptible error. A 40 mW/m^2 geotherm is also considered appropriate for concentrate from the Cleve-01 kimberlite (Wyatt *et al.*, 1994), implying that chromite-saturated garnet lherzolite occurs at P_{40} = 36·4 kbar (Table 2, Fig. 10). In the absence of concentrate garnets with materially higher Cr content, this real-pressure represents the deepest mantle material from Cleve-01, consistent with the absence of diamond at this locality.

Chromite-absent (minimum-pressure) barometry

The vast majority of garnet concentrates derived from kimberlite (or exploration samples) show little or no direct compositional evidence for Cr saturation. Our barometer can still be applied in this generalized circumstance *because Cr-pyrope compositions provide minimum-pressure estimates when chromite coexistence cannot be demonstrated* (Nickel, 1989). Thus chromite-absent diamond-associated garnets with ~5·0 wt % Cr_2O_3 plot at Cr contents below the GDC (open symbols in Fig. 4b) and return P_{38} values in the range 33–35 kbar, which can be reconciled with the presence of diamond only if the calculated pressures represent minima.

Our barometer is likely to find extensive application to garnet concentrate compositions where the highest Cr/Ca grain occurs in compositional isolation, and not associated with a chromite-saturated compositional array. We assign a chromite-absent status to such grains from the Koffiefontein and Nzega kimberlites (see Figs 9 and 11) and, assuming appropriate geothermal models, respectively calculate minimum pressures of P_{40} $\geq$45·1 kbar and P_{37} $\geq$34·7 kbar for them (Table 2). In this application the highest Cr/Ca grains provide estimates of the minimum thickness of depleted lithospheric material entrained by the kimberlite. Applying this concept to Cr-pyrope xenocrysts from kimberlites in central Quebec, Canada, we calculate the depleted lithosphere underlying the Portage area to extend across the range P_{38} $\geq$52·4 to 61·9 kbar, i.e. well into the diamond stability field on an assumed 38 mW/m^2 geotherm (Fig. 17a, Table 2). The Beaver Lake kimberlite occurs some 90 km to the south of the Portage area and provides evidence of depleted peridotite extending beyond P_{38} $\geq$42·0 kbar, based on the composition of a marginally lherzolitic Cr-pyrope xenocryst (Fig. 17b, Table 2); the actual lithosphere must extend deeper because trace diamond occurs at this locality (Girard, 2001).

Table 3: Maximum-value barometry results for a selection of cratonic settings

Region/cluster	Country	Setting	*n*	Cr_2O_3 (wt %)	CaO (wt %)	P_{38} (kbar)	Pressure (kbar)	Reference
Daldyn	Russia	Siberian craton, core	2604	13·69	3·07	61·7	P_{35} ≥62·8	Grütter *et al*. (1999, fig. 1e)
Daldyn	Russia	Siberian craton, core	>500	12·66	0·99	64·7	P_{35} ≥65·8	Ryan *et al*. (1996, fig. 2)
Shandong	China	East China craton, core	2996	14·55	2·88	65	P_{38} ≥65·0	Grütter *et al*. (1999, fig. 1d)
Hardy Lake	Canada	Slave craton, Central domain	1992	12·32	4·39	53·3	P_{36} ≥54·1	Grütter *et al*. (1999, fig. 2b)
Providence Lake	Canada	Slave craton, Central domain	3679	15·26	5·45	59·5	P_{36} ≥60·3	Grütter *et al*. (1999, fig. 2c)
Upper Carp Lake	Canada	Slave craton, Central domain	2048	13·89	4·13	59·1	P_{36} ≥59·9	Grütter *et al*. (1999, fig. 2d)
Gahcho Kue	Canada	Slave craton, Southern domain	3256	14·98	3·44	64·7	P_{36} ≥65·4	Grütter *et al*. (1999, fig. 2e)
Rocking Horse	Canada	Slave craton, Northern domain	2836	11·65	4·86	49·7	P_{36} ≥50·5	Grütter *et al*. (1999, fig. 2f)
Anuri	Canada	Slave craton, Northern domain	288	14·1	3·42	61·9	P_{36} ≥62·6	Masun *et al*. (2004, table 2)
Banankoro	Guinea	Man craton, core	10742	14·16	3·41	62·2	P_{40} ≥61·4	Skinner *et al*. (2004, fig. 15b)
Bouro	Guinea	Man craton, core	1787	14·35	4·84	58·4	P_{40} ≥57·6	Skinner *et al*. (2004, fig. 15a)
Koidu	Sierra Leone	Man craton, core	931	8·05	0·65	50·9	P_{40} ≥50·1	Skinner *et al*. (2004, fig. 15c)
Weasua	Liberia	Man craton, core	159	11·56	0·95	61·2	P_{40} ≥60·4	Skinner *et al*. (2004, fig. 15d)
Zero	South Africa	Kaapvaal craton, core	~300	9·72	2·77	49·8	P_{48} ≥45·9	Fig. 16, this work
Finsch	South Africa	Kaapvaal craton, core	664	10·7	2·92	52·5	P_{38} = 52·5	Fig. 7, this work
Kimberley	South Africa	Kaapvaal craton, core	~2500	10·18	1·44	55·3	P_{38} ≥55·3	Grütter *et al*. (1999, fig. 4d)
Sanddrift	South Africa	Kaapvaal craton, inboard edge	~2500	8·15	1·54	48·5	P_{38} ≥48·5	Grütter *et al*. (1999, fig. 4c)
Marydale	South Africa	Kaapvaal craton, outboard edge	~2500	6·78	0·76	46·4	P_{40} ≥45·6	Grütter *et al*. (1999, fig. 4b)
Namaqua	South Africa	Proterozoic, off craton	~2500	9·46	3·56	46·6	P_{44} ≥44·3	Grütter *et al*. (1999, fig. 4a)
State Line	USA	Wyoming craton, inboard edge	2257	15·63	7·93	53·2	P_{41} ≥52·0	Grütter *et al*. (1999, fig. 1c)
Gibeon	Namibia	Proterozoic, off craton	2558	8·99	5·54	39·6	P_{44} ≥37·3	Grütter *et al*. (1999, fig. 1b)

Maximum-value barometry to establish lithosphere depth

The examples outlined above demonstrate that the maximum value obtained during general application of the minimum-pressure barometer depends critically on the prevalence of high-Cr/Ca garnets in a concentrate, particularly those related to harzburgite (Figs 9, 11 and 17). The incidence of such garnet compositions in a dataset is in turn related to the colour representation and quantity of concentrate garnets analysed, the distribution of harzburgitic or Cr-rich lherzolitic bulk compositions at depth within the lithosphere, and the vagaries of how such mantle rock types are entrained by, and disaggregate within, kimberlite magmas. Real-pressure barometry is not possible in the absence of evidence of Cr saturation (e.g. Figs 4–11), and estimates of the depth extent of depleted lithosphere should rely on procurement of several hundred to thousands of garnet analyses that represent a cluster of spatially related kimberlites. Examples of maximum-value depth constraints provided by such densely populated 'mature' datasets are listed in Table 3 and are briefly discussed below.

Our barometer shows Cr-rich peridotite to occur at depths of at least 60–65 kbar in the central portions of the East China, Siberian, Slave and the West African Man cratons (Table 3). Although minimum pressures for extreme high-Cr/Ca garnets from Daldyn (Russia) and Gahcho Kue (southern Slave) approach 66 kbar, there is no evidence of Cr-rich, depleted lithosphere at depths of 70 kbar (Table 3), implying that it does not exist at such pressures, or that kimberlite magmas cannot entrain depleted peridotite from such depths. However, conventional thermobarometry results document derivation of garnet peridotite xenoliths from 65–70 kbar in the Daldyn, Northern Slave and Southern Slave regions (Griffin *et al*., 1996; Kopylova *et al*., 1999; Koplova & Caro, 2004), providing reassurance that application of maximum-value Cr barometry to 'mature' datasets yields robust estimates of the depth extent of Cr-rich, depleted lithosphere.

The western portion of the Kaapvaal craton is richly endowed with numerous and diverse kimberlite magma types that occur in an ~450 km long traverse stretching from Kimberley across the craton margin to the off-craton, Proterozoic Namaqualand Metamorphic Complex (Skinner *et al*., 1994; Grütter *et al*., 1999). Cr-pyrope concentrates from these kimberlites show depleted peridotite to occur at ~53 kbar in the Finsch area (Fig. 7, Table 2), ~55 kbar in the Kimberley area (Table 3) and ~53 kbar in the vicinity of Roberts Victor, located some 80 km ENE of Kimberley (Table 2). These

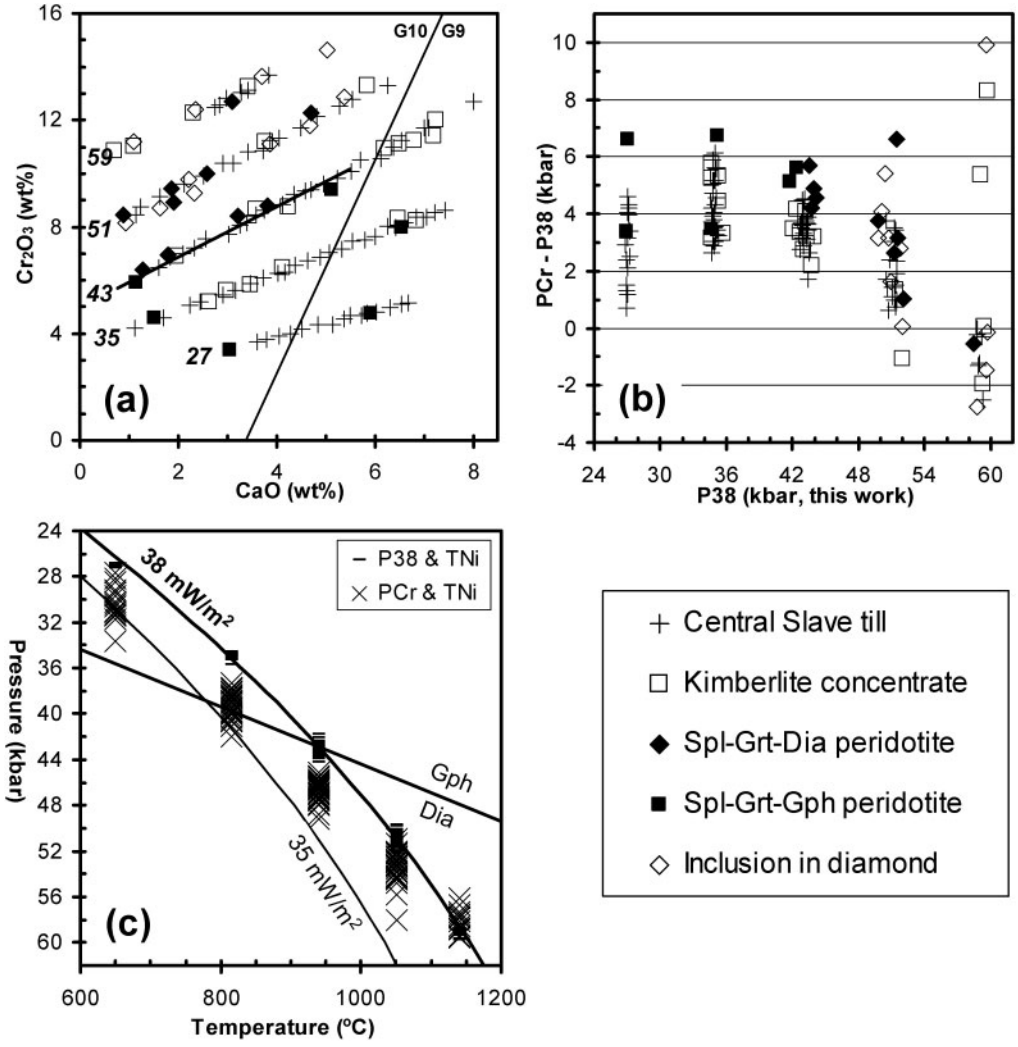

Fig. 18. Comparison of P_{Cr} (Ryan *et al.*, 1996) and P_{38} (this work) barometer results for garnets compositions at nominal P_{38} values of 27, 35, 43, 51 and 59 kbar (a) from a variety of sources (legend). The $P_{Cr} - P_{38}$ difference (b) shows $P_{Cr} > P_{38}$ in general, but $P_{Cr} \leq P_{38}$ at high pressure. The P_{Cr} barometer consequently underestimates a 38 mW/m^2 geotherm by ~2 mW/m^2 compared with the P_{38} formulation, except at high pressure (c). Three low-Ca points plot off-scale at 64–70 kbar in (c). (See Fig. 19 and text for further discussion.) All garnet compositions, P_{38} and P_{Cr} results are given as supplementary data (Electronic Appendix 2).

maximum-value barometry results suggest that the depleted lithosphere underlying the diamond mines in the western Kaapvaal craton is significantly thinner than the mantle roots of many other Archaean cratons. The available data support thinning of the Kaapvaal lithosphere to depths equivalent to pressures of ~49 kbar at the inboard edge of the craton, and only ~46 kbar underlying the Marydale domain along the outboard edge of the craton (Table 3; Grütter *et al.*, 1999, fig. 4b). Peridotitic mantle material beneath the off-craton Namaqua and Gibeon kimberlite provinces is dominated by moderately depleted lherzolitic bulk compositions, which evidently do not extend beyond depths equivalent to pressures of ~45 and ~38 kbar, respectively (Table 3). The off-craton lithospheric sections thus fall within the graphite stability field assuming a 44 mW/m^2 geotherm applies, consistent with the diamond-absent status of kimberlites in the Namaqua and Gibeon provinces.

Comparison with the P_{Cr} barometer of Ryan *et al.* (1996)

A comparison of typical results for the P_{38} (this work) and P_{Cr} (Ryan *et al.*, 1996) barometer formulations is presented in Figs 18 and 19. Garnet compositions falling at nominal P_{38} values of 27, 35, 43, 51 and 59 kbar were selected from (1) open-file data for diamond exploration till samples from the central Slave craton (n = 86, Armstrong, 2001); (2) concentrate from Slave craton kimberlites (n = 20, mostly from Griffin *et al.*, 2004);

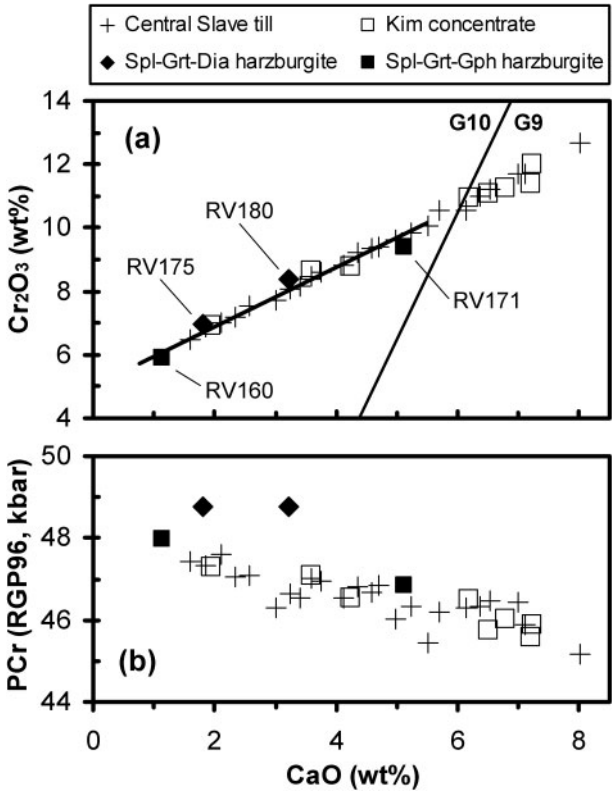

Fig. 19. Input compositions (a) and results (b) for P_{Cr} barometry (Ryan *et al.*, 1996) with GDC-like garnet compositions from various sources (legend). Filled symbols denote harzburgite xenoliths that pin the graphite–diamond transition to 43 kbar, 940°C at Roberts Victor [based on Kennedy & Kennedy (1976)]. However, P_{Cr} calculations assuming $T_{Ni} = 940$°C (i.e. 37 ppm Ni) yield pressures of 45–49 kbar, considerably greater than 43 kbar. All garnet compositions, P_{38} and P_{Cr} results are given as supplementary data (Electronic Appendix 2).

(3) inclusions in diamonds ($n = 11$, several sources) and (4) chromite-saturated garnet peridotites with graphite or diamond ($n = 16$, a subset of data in Electronic Appendix 1). P_{38} and P_{Cr} values were calculated assuming equilibration of garnet with chromite, orthopyroxene and olivine at temperatures along a 38 mW/m^2 conductive geotherm. The comparison is therefore made at nominal P–T (kbar–°C) of 27–650, 35–815, 43–940, 51–1050 and 59–1140 for a range of garnet Cr_2O_3–CaO compositions (Fig. 18a), thereby replicating the P–T–X conditions inherent in the P_{38} calibration of this work. All compositional data, data sources and thermobarometry results are provided as supplementary data (Electronic Appendix 2, available at http://www.petrology.oxfordjournals.org).

Our thermobarometry results show $P_{Cr} > P_{38}$ in general, but $P_{Cr} \leq P_{38}$ at very high Cr content (Fig. 18b). The P_{Cr} and P_{38} formulations generally agree to within 2 kbar for a limited pressure range at 55 ± 2 kbar, but P_{Cr} yields 5 to ~7 kbar higher pressures than P_{38} for all very low-Ca compositions (those with CaO <1·2 wt %; Fig. 18a and b, and Electronic Appendix 2). Excluding these low-Ca data, we find that P_{Cr} typically yields 7–10% higher pressures than P_{38} at 27 kbar < P_{38} < 53 kbar, this being a mantle interval commonly sampled by diamondiferous kimberlites. The combination of P_{Cr} with T_{Ni} for pyrope garnet (Ryan *et al.*, 1996) would therefore typically underestimate mantle geotherms compared with a P_{38}–T_{Ni} combination. Figure 18c shows the underestimate to amount to ~2 mW/m^2 on average for cool, cratonic geotherms, though earlier modelling indicates a larger underestimate occurs for hot geotherms (see Grütter & Sweeney, 2000).

The GDC provides an additional opportunity to compare results for the P_{38} and P_{Cr} barometers. On assuming Cr-saturated conditions in an orthopyroxene–olivine assemblage, both barometers should reproduce a pressure of ~43 kbar at a temperature of 940°C when applied to GDC-like garnet compositions. Our calculations (Electronic Appendix 2) show that P_{Cr} systematically overestimates pressure by ~6–12% at these conditions and illustrate an unresolved inverse dependence of P_{Cr} on garnet CaO content (Fig. 19b). We conclude that the barometer formulated in this work yields substantially different results from the P_{Cr} barometer of Ryan *et al.* (1996), for common cratonic geothermal gradients and the range of Cr-pyrope compositions that characteristically occur in heavy mineral concentrates from kimberlite.

SUMMARY AND CONCLUSION

Our empirical analysis of Cr-pyrope compositions in heavy mineral concentrates from kimberlite shows chromite saturation in natural harzburgite and lherzolite to be expressed as linear arrays with Cr_2O_3/CaO near unity in garnet Cr_2O_3 vs CaO diagrams (Figs 4–13). When conceptualized as pressure increments along a standard-state conductive mantle geotherm, a 38 mW/m^2 model being chosen in this work, the arrays may be used as a graphical template (Fig. 14) to calibrate a simple, effective Cr/Ca-in-garnet barometer (Fig. 15) with low, negative temperature dependence (Fig. 16). Our P_{38} barometer formulation is internally consistent with Cr-saturated garnet compositions in cratonic harzburgite and lherzolite assemblages and is closely constrained at the graphite–diamond transition (Fig. 4), which roughly bisects the calibrated compositional range (Fig. 15). We anticipate general application of the barometer to xenocrystic Cr-pyrope compositions derived from kimberlite, for which minimum entrainment depths can be estimated (e.g. Fig. 17). The maximum depth obtained approaches the base of the Cr/Al-enriched, depleted lithosphere with increased maturity in the number and diversity of xenocryst sources considered (Table 3). The P_{Cr} barometer of

Ryan *et al.* (1996) cannot reproduce the compositional and P–T constraints of our P_{38} formulation (Fig. 18) and we conclude that our empirical barometer is preferred for all situations where conductive geotherms intersect the graphite–diamond equilibrium (Figs 16 and 19).

ACKNOWLEDGEMENTS

We thank Gerhard Brey and Andrei Girnis for informative discussions on spinel–garnet relations in peridotites and gratefully acknowledge the contribution made by numerous researchers who painstakingly documented assemblages and mineral compositions in carbon-bearing peridotite xenoliths. The De Beers Group of Companies and Mineral Services is acknowledged for support during various stages of this project and for facilitating access to critical concentrate datasets. H.S.G. publishes with permission of De Beers Consolidated Mines Limited. Journal reviews by Gerhard Brey, Dante Canil and Bill Griffin markedly improved the presentation and overall clarity of the manuscript.

SUPPLEMENTARY DATA

Supplementary data for this paper are available at *Journal of Petrology* online.

REFERENCES

Armstrong, J. P. (2001). Kimberlite Indicator Mineral Chemistry Database (KIMC): a preliminary digital compilation of Kimberlite Indicator Mineral Chemistry extracted from publicly available assessment filings; Slave craton and environs, Northwest Territories and Nunavut, Canada. DIAND NWT Geology Division, EGS Open Report 2001-02 (CD-ROM).

Bell, D. R., Schmitz, M. D. & Janney, P. E. (2003). Mesozoic thermal evolution of the Southern African mantle lithosphere. *Lithos* **71**, 273–287.

Bence, A. E. & Albee, A. L. (1968). Empirical correction factors for the electron microanalysis of silicates and oxides. *Journal of Geology* **76**, 382–403.

Brey, G. P., Doroshev, A. M. & Kogarko, L. (1991). The join pyrope–knorringite: experimental constraints for a new geothermobarometer for coexisting garnet and spinel. *Extended Abstracts, 5th International Kimberlite Conference*, 24–28 June 1991, pp. 26–28.

Brey, G. P., Doroshev, A. M., Girnis, A. V. & Turkin, A. I. (1999). Garnet–spinel–olivine–orthopyroxene equilibria in the FeO–MgO–Al_2O_3–SiO_2–Cr_2O_3 system: I. Composition and molar volumes of minerals. *European Journal of Mineralogy* **11**, 599–617.

Burgess, S. R. & Harte, B. (1999). Tracing lithosphere evolution through the analysis of heterogeneous G9/G10 garnets in peridotite xenoliths, I: major element chemistry. In: Gurney, J. J., Gurney, J. L., Pascoe, M. D. & Richardson, S. H. (eds) *Proceedings of the 7th International Kimberlite Conference*. Cape Town: Red Roof Design, pp. 66–80.

Carbno, G. B. & Canil, D. (2002). Mantle structure beneath the SW Slave Craton, Canada: constraints from garnet geochemistry in the Drybones Bay kimberlite. *Journal of Petrology* **43**, 129–142.

Chatterjee, N. D. & Terhart, L. (1985). Thermodynamic calculation of peridotite phase relations in the system MgO–Al_2O_3–SiO_2–Cr_2O_3, with some geological applications. *Contributions to Mineralogy and Petrology* **89**, 273–284.

Dawson, J. B., Smith, J. V. & Delaney, J. S. (1978). Multiple spinel–garnet peridotite transitions in upper mantle: evidence from a harzburgite xenolith. *Nature* **273**, 741–743.

Doroshev, A. M., Brey, G. P., Girnis, A. V., Turkin, A. I. & Kogarko, L. N. (1997). Pyrope–knorringite garnets in the Earth's upper mantle: experiments in the MgO–Al_2O_3–SiO_2–Cr_2O_3 system. *Russian Geology and Geophysics* **38**, 559–586.

Field, S. W. & Haggerty, S. E. (1994). Symplectites in upper mantle peridotites: development and implications for the growth of subsolidus garnet, pyroxene and spinel. *Contributions to Mineralogy and Petrology* **118**, 138–156.

Finnerty, A. A. & Boyd, F. R. (1987). Thermobarometry for garnet peridotite xenoliths: a basis for the thermal and compositional structure of the upper mantle. In: Nixon, P. H. (ed.) *Mantle Xenoliths*. New York: John Wiley, pp. 381–402.

Fursenko, B. A. (1981). Synthesis of new high pressure garnets: $Mn_3Cr_2Si_3O_{12}$ and $Fe_3Cr_2Si_3O_{12}$. *Bulletin de Minéralogie* **104**, 418–422.

Gasparik, T. (1987). Orthopyroxene thermobarometry in simple and complex systems. *Contributions to Mineralogy and Petrology* **96**, 357–370.

Gasparik, T. (2000). An internally consistent thermodynamic model for the system CaO–MgO–Al_2O_3–SiO_2 derived primarily from phase equilibrium data. *Journal of Geology* **108**, 103–119.

Girard, R. (2001). Caractérisation de l'intrusion kimberlitique du lac Beaver, Monts Otish—pétrographie et minéralogie. Ressources Naturelles Quebec, Report MB2001-08, 23 pp. (in French).

Girnis, A. V. & Brey, G. P. (1999). Garnet–spinel–olivine–orthopyroxene equilibria in the FeO–MgO–Al_2O_3–SiO_2–Cr_2O_3 system: II. Thermodynamic analysis. *European Journal of Mineralogy* **11**, 619–636.

Girnis, A. V., Stachel, T., Brey, G. P., Harris, J. W. & Phillips, D. (1999). Internally consistent geothermobarometers for garnet harzburgites: model refinement and application. In: Gurney, J. J., Gurney, J. L., Pascoe, M. D. & Richardson, S. H. (eds) *Proceedings of the 7th International Kimberlite Conference*. Cape Town: Red Roof Design, pp. 247–254.

Girnis, A. V., Brey, G. P., Doroshev, A. M., Turkin, A. I. & Simon, N. (2003). The system MgO–Al_2O_3–SiO_2–Cr_2O_3 revisited: reanalysis of Doroshev *et al.*'s (1997) experiments and new experiments. *European Journal of Mineralogy* **15**, 953–964.

Green, D. H. & Ringwood, A. E. (1970). Mineralogy of peridotitic compositions under upper mantle conditions. *Physics of the Earth and Planetary Interiors* **3**, 359–371.

Griffin, W. L. & Ryan, C. G. (1995). Trace elements in indicator minerals: area selection and target evaluation in diamond exploration. *Journal of Geochemical Exploration* **53**, 311–337.

Griffin, W. L., Gurney, J. J. & Ryan, C. G. (1992). Variations in trapping temperatures and trace elements in peridotite-suite inclusions from African diamonds: evidence for two inclusion suites, and implications for lithosphere stratigraphy. *Contributions to Mineralogy and Petrology* **110**, 1–15.

Griffin, W. L., Sobolev, N. V., Ryan, C. G., Pokhilenko, N. P., Win, T. T. & Yefimova, E. S. (1993). Trace elements in garnets and chromites: diamond formation in the Siberian lithosphere. *Lithos* **29**, 235–256.

Griffin, W. L., Kaminsky, F. V., Ryan, C. G., O'Reilly, S. Y., Win, T. T. & Ilupin, I. P. (1996). Thermal state and composition of the lithospheric mantle beneath the Daldyn kimberlite field, Yakutia. *Tectonophysics* **262**, 19–33.

Griffin, W. L., Fisher, N. I., Friedman, J. H., Ryan, C. G. & O'Reilly, S. Y. (1999). Cr-pyrope garnets in the lithospheric mantle I. Compositional systematics and relations to tectonic setting. *Journal of Petrology* **40**, 679–704.

Griffin, W. L., O'Reilly, S. Y., Natapov, L. M. & Ryan, C. G. (2003). The evolution of lithospheric mantle beneath the Kalahari craton and its margins. *Lithos* **71**, 215–241.

Griffin, W. L., O'Reilly, S. Y., Doyle, B. J., Pearson, N. J., Coopersmith, H., Malkovets, V. & Pokhilenko, N. (2004). Lithosphere mapping beneath the North American plate. *Lithos* **77**, 873–922.

Grütter, H. S. (1994). Spinel–garnet–carbon phase relations in coarse Kaapvaal-type peridotites and implications for garnet–orthopyroxene equilibration. *Extended Abstracts, International Symposium on the Physics and Chemistry of the Upper Mantle*, São Paulo, June 1994, pp. 5–7.

Grütter, H. S. & Sweeney, R. J. (2000). Tests and constraints on single-grain Cr-pyrope barometer models: some initial results. *Extended Abstracts, GeoCanada 2000: The Millenium Geoscience Summit*, 29 May–2 June 2000, Calgary, Abstract 772, 4 pp. (on CD-ROM).

Grütter, H. S., Apter, D. B. & Kong, J. (1999). Crust–mantle coupling: evidence from mantle-derived xenocrystic garnets. In: Gurney, J. J., Gurney, J. L., Pascoe, M. D. & Richardson, S. H. (eds) *Proceedings of the 7th International Kimberlite Conference*. Cape Town: Red Roof Design, pp. 307–313.

Grütter, H. S., Gurney, J. J., Menzies, A. H. & Winter, F. (2004). An updated classification scheme for mantle-derived garnet, for use by diamond explorers. *Lithos* **77**, 841–857.

Gurney, J. J. (1984). A correlation between garnets and diamonds. In: Glover, J. E. & Harris, P. G. (eds) *Kimberlite Occurrence and Origin: a Basis for Conceptual Models in Exploration. Geology Department and University Extension, University of Western Australia Publication* **8**, 143–166.

Gurney, J. J. & Switzer, G. S. (1973). The discovery of garnets closely related to diamonds in the Finsch pipe, South Africa. *Contributions to Mineralogy and Petrology* **39**, 103–116.

Harley, S. L. (1984). An experimental study of the partitioning of Fe and Mg between garnet and orthopyroxene. *Contributions to Mineralogy and Petrology* **86**, 359–373.

Harris, J. (1992). Diamond geology. In: Field, J. E. (ed.) *The Properties of Natural and Synthetic Diamond*. London: Academic Press, pp. 345–393.

Harte, B. & Hawkesworth, C. J. (1989). Mantle domains and mantle xenoliths. In: Ross, J. (ed.) *Kimberlites and Related Rocks. Geological Society of Australia Special Publication* **14**, 649–686.

Ionov, D. A., Ashchepkov, I. V., Stosch, H.-G., Witt-Eickschen, G. & Seck, H. A. (1993). Garnet peridotite xenoliths from the Vitim volcanic field, Baikal region: the nature of the garnet–spinel peridotite transition zone in the continental mantle. *Journal of Petrology* **34**, 1141–1175.

Irifune, T. (1985). Experimental study of the system $Mg_3Al_2Si_3O_{12}$–$Mg_3Cr_2Si_3O_{12}$ at high pressure and high temperature. *Journal of the Faculty of Science, Hokkaido University (Series IV)* **21**, 417–451.

Irifune, T., Ohtani, E. & Kumazawa, M. (1982). Stability field of knorringite $Mg_3Cr_2Si_3O_{12}$ at high pressure and its implication to the occurrence of Cr-rich pyrope in the upper mantle. *Physics of the Earth and Planetary Interiors* **27**, 263–272.

Kennedy, C. S. & Kennedy, G. C. (1976). The equilibrium boundary between graphite and diamond. *Journal of Geophysical Research* **81**, 2467–2470.

Klemme, S. (2004). The influence of Cr on the garnet–spinel transition in the Earth's mantle: experiments in the system MgO–Cr_2O_3–SiO_2 and thermodynamic modeling. *Lithos* **77**, 639–646.

Klemme, S. & O'Neill, H. S. C. (2000). The effect of Cr on the solubility of Al in orthopyroxene: experiments and thermodynamic modelling. *Contributions to Mineralogy and Petrology* **140**, 84–98.

Kopylova, M. G. & Caro, G. (2004). Mantle xenoliths from the southeastern Slave craton: evidence for chemical zonation in a thick, cold lithosphere. *Journal of Petrology* **45**, 1045–1067.

Kopylova, M. G., Gurney, J. J. & Daniels, L. R. M. (1997). Mineral inclusions in diamonds from the River Ranch kimberlite, Zimbabwe. *Contributions to Mineralogy and Petrology* **129**, 366–384.

Kopylova, M. G., Russell, J. K. & Cookenboo, H. (1999). Petrology of peridotite and pyroxenite xenoliths from the Jericho kimberlite: implications for the thermal state of the mantle beneath the Slave craton, Northern Canada. *Journal of Petrology* **40**, 79–104.

Kopylova, M. G., Russell, J. K., Stanley, C. & Cookenboo, H. (2000). Garnet from Cr- and Ca-saturated mantle: implications for diamond exploration. *Journal of Geochemical Exploration* **68**, 183–199.

Lehtonen, M. L., O'Brien, H. E., Peltonen, P., Johanson, B. S. & Pakkanen, L. K. (2004). Layered mantle at the Karelian Craton margin: *P–T* of mantle xenocrysts and xenoliths from the Kaavi–Kuopio kimberlites, Finland. *Lithos* **77**, 593–608.

MacGregor, I. D. (1965). Stability fields of spinel and garnet peridotites in the synthetic system MgO–CaO–Al_2O_3–SiO_2. *Carnegie Institute of Washington Yearbook* **64**, 126–134.

MacGregor, I. D. (1970). The effect of CaO, Cr_2O_3, Fe_2O_3 and Al_2O_3 on the stability of spinel and garnet peridotites. *Physics of the Earth and Planetary Interiors* **3**, 372–377.

Malinovsky, I. Y. & Doroshev, A. M. (1975). Effect of temperature and pressure on the composition of Cr-bearing phases of the garnet + enstatite + spinel + forsterite associations. In: *Experimental Research on Mineralogy. Bulletin Institute Geology and Geophysics, Novosibirsk*, pp. 121–125 (in Russian).

Malinovsky, I. Y. & Doroshev, A. M. (1977). Evaluation of *P–T* conditions of diamond formation with reference to chrome-bearing garnet stability. *Extended Abstracts, 2nd International Kimberlite Conference*, Santa Fe, N.M., unpaginated.

Masun, K. M., Doyle, B. J., Ball, S. & Walker, S. (2004). The geology and mineralogy of the Anuri kimberlite, Nunavut, Canada. *Lithos* **76**, 75–97.

Menzies, A. H. (2001). A detailed investigation into diamond-bearing xenoliths from Newlands kimberlite, South Africa. Ph.D. thesis, University of Cape Town, 253 pp.

Menzies A. H., Shirey, S. B., Carlson, R. W. & Gurney, J. J. (1999). Re–Os systematics of Newlands peridotite xenoliths: implications for diamond and lithosphere formation. In: Gurney, J. J., Gurney, J. L., Pascoe, M. D. & Richardson, S. H. (eds) *Proceedings of the 7th International Kimberlite Conference*. Cape Town: Red Roof Design, pp. 566–583.

Nickel, K. G. (1986). Phase equilibria in the system SiO_2–MgO–Al_2O_3–CaO–Cr_2O_3 (SMACCR) and their bearing on spinel/garnet lherzolite relationships. *Neues Jahrbuch für Mineralogie, Abhandlungen* **155**, 259–287.

Nickel, K.G. (1989). Garnet–pyroxene equilibria in the system SMACCR (SiO_2–MgO–Al_2O_3–CaO–Cr_2O_3): the Cr-geobarometer. In: Ross, J. (ed.) *Kimberlites and Related Rocks. Geological Society of Australia Special Publication* **14**, 901–912.

Nimis, P. (1998). Evaluation of diamond potential from the composition of peridotitic chromian diopside. *European Journal of Mineralogy* **10**, 505–519.

Nimis, P. & Taylor, W. R. (2000). Single clinopyroxene thermobarometry for garnet peridotites. Part 1. Calibration and testing of a Cr-in-cpx barometer and enstatite-in-cpx thermometer. *Contributions to Mineralogy and Petrology* **139**, 541–554.

O'Hara, M. J., Richardson, S. W. & Wilson, G. (1971). Garnet peridotite stability and occurrence in crust and mantle. *Contributions to Mineralogy and Petrology* **32**, 48–68.

O'Neill, H. St. C. (1981). The transition between spinel lherzolite and garnet lherzolite, and its use as a geobarometer. *Contributions to Mineralogy and Petrology* **77**, 185–194.

O'Neill, H. S. C. & Wood, B. J. (1979). An experimental study of Fe–Mg partitioning between garnet and olivine and its calibration as a geothermometer. *Contributions to Mineralogy and Petrology* **70**, 59–70.

Pollack, H. N. & Chapman, D. S. (1977). On the regional variation of heat flow, geotherms, and lithospheric thickness. *Tectonophysics* **38**, 279–296.

Rickard, R. S., Harris, J. W., Gurney, J. J. & Cardoso, P. (1986). Mineral inclusions in diamonds from Koffiefontein mine. In: Ross, J. (ed.) *Kimberlites and Related Rocks. Geological Society of Australia Special Publication* **14**, 1054–1062.

Robinson, J. A. C. & Wood, B. J. (1998). The depth of the garnet/spinel transition in fractionally melting peridotite. *Earth and Planetary Science Letters* **164**, 277–284.

Ryan, C. G., Griffin, W. L. & Pearson, N. J. (1996). Garnet geotherms: pressure–temperature data from Cr-pyrope garnet xenocrysts in volcanic rocks. *Journal of Geophysical Research* **101**, 5611–5625.

Sage, R. P. (2000). Kimberlites of the Attawapiskat area, James Bay lowlands, northern Ontario. Ontario Geological Survey Open File Report 6019, 341 pp.

Schulze, D. J. (1995). Low-Ca garnet harzburgites from Kimberley, South Africa: abundance and bearing on the structure and evolution of the lithosphere. *Journal of Geophysical Research* **100**, 12513–12526.

Schulze, D. J. (1996). Chromite macrocrysts from southern African kimberlites: mantle xenolith sources and post-diamond re-equilibration. In: Kogbe, C. A. (ed.) *Diamond Deposits in Africa. Special Issue Africa Geoscience Review* **3**, 203–216.

Shee, S. R., Gurney, J. J. & Robinson, D. N. (1982). Two diamond-bearing peridotite xenoliths from the Finsch kimberlite, South Africa. *Contributions to Mineralogy and Petrology* **81**, 79–87.

Shee, S. R., Bristow, J. W., Bell, D. R., Smith, C. B., Allsopp, H. L. & Shee, P. B. (1989). The petrology of kimberlites, related rocks and associated mantle xenoliths from the Kuruman province, South Africa. In: Ross, J. (ed.) *Kimberlites and Related Rocks. Geological Society of Australia Special Publication* **14**, 60–82.

Skewes, M. A. & Stern, C. R. (1979). Petrology and geochemistry of alkali basalts and ultramafic inclusions from the Palei-Aike volcanic field in southern Chile and the origin of the Patagonian plateau lavas. *Journal of Volcanology and Geothermal Research* **6**, 3–25.

Skinner, C. P. (1989). The petrology of peridotite xenoliths from the Finsch kimberlite, South Africa. *South African Journal of Geology* **92**, 197–206.

Skinner, E. M. W., Smith C. B., Viljoen, K. S. & Clark, T. C. (1994). The petrography, tectonic setting and emplacement ages of kimberlites in the south western border region of the Kaapvaal craton, Prieska area, South Africa. In: Meyer, H. O. & Leonardos, O. H. (eds) *Kimberlites, Related Rocks and Mantle Xenoliths. CPRM Special Publication* **1A**, 80–95.

Skinner, E. M. W., Apter, D. B., Morelli, C. & Smithson, N. K. (2004). Kimberlites of the Man craton, West Africa. *Lithos* **76**, 233–259.

Smith, D. & Wilson, C. R. (1985). Garnet–olivine equilibration during cooling in the mantle. *American Mineralogist* **70**, 30–39.

Sobolev, N. V., Lavrent'ev, Y. G., Pokhilenko, N. P. & Usova, L. V. (1973). Chrome-rich garnets from the kimberlites of Yakutia and their paragenesis. *Contributions to Mineralogy and Petrology* **40**, 39–52.

Sobolev, N. V., Botkunov, A. I., Lavrent'ev, Y. G. & Usova, L. V. (1976). New data on mineral compositions as coexisting with diamonds of kimberlite pipe 'Mir' (Yakutia). *Geologiya i Geofizika* **12**, 3–15 (in Russian).

Sobolev, N. V., Pokhilenko, N. P. & Yefimova, E. S. (1984). Diamond-bearing peridotite xenoliths in kimberlites and the problem of the origin of diamonds. *Russian Geology and Geophysics* **25**, 63–80.

Sobolev, N. V., Pokhilenko, N. P. & Afanas'ev, V. P. (1993). Kimberlitic pyrope and chromite morphology and chemistry, as indicators of diamond grade in Yakutian and Arkhangelsk provinces. In: Dunne, K. P. E. & Grant, B. (eds) *Mid-Continent Diamonds. GAC–MAC Symposium Abstracts*, Edmonton, June 1993, pp. 63–69.

Sobolev, N. V., Yefimova, E. S., Reimers, L. F., Zakharchenko, O. D., Makhin, A. I. & Usova, L. V. (1997). Mineral inclusions in diamonds of the Arkhangelsk kimberlite province. *Russian Geology and Geophysics* **38**, 379–393.

Stachel, T., Viljoen, K. S., Brey, G. & Harris, J. W. (1998). Metasomatic processes in lherzolitic and harzburgitic domains of diamondiferous lithospheric mantle: REE in garnets from xenoliths and inclusions in diamonds. *Earth and Planetary Science Letters* **159**, 1–12.

Stern, C. R., Saul, S., Skewes, M. A. & Futa, K. (1986). Garnet peridotite xenoliths from the Pali-Aike alkali basalts of southernmost South America. In: Ross, J. (ed.) *Kimberlites and Related Rocks. Geological Society of Australia Special Publication* **14**, 736–744.

Stiefenhofer, J., Viljoen, K. S., Tainton, K. M., Dobbe, R. & Hannweg, G. W. (1999). The petrology of a mantle xenolith suite from Venetia, South Africa. In: Gurney, J. J., Gurney, J. L., Pascoe, M. D. & Richardson, S. H. (eds) *Proceedings of the 7th International Kimberlite Conference*. Cape Town: Red Roof Design, pp. 836–845.

Tainton, K. M., Seggie, A. G., Bayly, B. A., Tomlinson, I. & Quadling, K. E. (1999). Garnet thermobarometry: implications for mantle heat flow within the Tanzanian craton. In: Gurney, J. J., Gurney, J. L., Pascoe, M. D. & Richardson, S. H. (eds) *Proceedings of the 7th International Kimberlite Conference*. Cape Town: Red Roof Design, pp. 852–860.

Viljoen, K. S., Robinson, D. N., Swash, P. M., Griffin, W. L., Otter, M. L., Ryan, C. G. & Win, T. T. (1994). Diamond- and graphite-bearing peridotite xenoliths from the Roberts Victor kimberlite, South Africa. In: Meyer, H. O. & Leonardos, O. H. (eds) *Kimberlites, Related Rocks and Mantle Xenoliths. CPRM Special Publication* **1A**, 285–303.

Webb, S. A. C. & Wood, B. J. (1986). Spinel–pyroxene–garnet relationships and their dependence on Cr/Al ratio. *Contributions to Mineralogy and Petrology* **92**, 471–480.

Wood, B. J. & Fraser, D. G. (1976). *Elementary Thermodynamics for Geologists*. Oxford: Oxford University Press, 303 pp.

Woodland, A. B. & O'Neill, H. St. C. (1995). Phase relations between $Ca_3Fe_2Si_3O_{12}$–$Fe_3Fe_2Si_3O_{12}$ garnet and $CaFeSi_2O_6$–$Fe_2Si_2O_6$ pyroxene solid solutions. *Contributions to Mineralogy and Petrology* **121**, 87–98.

Wyatt, B. A., Shee, S. R., Griffin, W. L., Zweistra, P. & Robison, H. R. (1994). The petrology of the Cleve kimberlite, Eyre peninsula, South Australia. In: Meyer, H. O. & Leonardos, O. H. (eds) *Kimberlites, Related Rocks and Mantle Xenoliths. CPRM Special Publication* **1A**, 62–79.